Molecular Therapy
Methods & Clinical Development
Original Article

miR-195 Has a Potential to Treat Ischemic and Hemorrhagic Stroke through Neurovascular Protection and Neurogenesis

Hsin-Yun Cheng,[1,10] Yung-Song Wang,[1,2,3,10] Po-Yuan Hsu,[1,4] Chien-Yuan Chen,[1,4] Yi-Chu Liao,[5,6] and Suh-Hang H. Juo[4,7,8,9]

[1]Department of Genome Medicine, College of Medicine, Kaohsiung Medical University, 100, Shih-Chuan 1st Road, Kaohsiung 807, Taiwan; [2]Institute of Fisheries Science, National Taiwan University, 1, Sec. 4, Roosevelt Road, Taipei 10617, Taiwan; [3]Department of Life Science, National Taiwan University, 1, Sec. 4, Roosevelt Road, Taipei 10617, Taiwan; [4]Department of Medical Research, China Medical University Hospital, 2 Yude Road, Taichung, 40447, Taiwan; [5]Department of Neurology, National Yang-Ming University School of Medicine, Taipei, Taiwan; [6]Department of Neurology, Taipei Veterans General Hospital, No. 201, Sec. 2, Shipai Road, Taipei 112, Taiwan; [7]Graduate Institute of Biomedical Sciences, China Medical University, 91 Hsueh-Shih Road, Taichung 40402, Taiwan; [8]Institute of New Drug Development, China Medical University, 91 Hsueh-Shih Road, Taichung 40402, Taiwan; [9]Drug Development Center, China Medical University, Taichung, Taiwan

Tissue plasminogen activator is the only U.S. FDA-approved therapy for ischemic stroke, while there is no specific medication for hemorrhagic stroke. Therefore, the treatment of acute stroke continues to be a major unmet clinical need. We explored the effects of miR-195 on neurovascular protection and its potential in treating acute stroke. Using both cellular and animal studies, we showed that miR-195's beneficial effects are mediated by four mechanisms: (1) anti-apoptosis for injured neural cells by directly suppressing Sema3A/Cdc42/JNK signaling, (2) neural regeneration by promoting neural stem cell proliferation and migration, (3) anti-inflammation by directly blocking the NF-kB pathway, and (4) improvement of endothelial functions. We intravenously injected miR-195 carried by nanoparticles into rats with either ischemic or hemorrhagic stroke in the acute stage. The results showed that miR-195 reduced the size of brain damage and improved functional recovery in both types of stroke rats. The reduction of injured brain volume could be up to 45% in ischemic stroke and approximately 30% in hemorrhagic stroke. The therapeutic window between stroke onset and miR-195 treatment could be up to 6 h. Our data demonstrated that miR-195 possesses the potential to become a new drug to treat acute ischemic and hemorrhagic stroke.

INTRODUCTION

Stroke is a leading cause of death and disability worldwide. Stroke can be characterized as ischemic or hemorrhagic, with ischemic stroke accounting for 85% of instances.[1] The intravenous administration of tissue plasminogen activator (tPA) within 3 h of stroke onset, and within 4.5 h of stroke onset in select patients,[2] is currently the only U.S. Food and Drug Administration (FDA)-approved therapy for ischemic stroke. Because of the time-dependent nature of tPA therapy and a fear of hemorrhagic complications, only 1%–8% of potentially eligible patients have been treated with tPA.[3] In contrast to treatment for ischemic stroke, the recommendation for managing hemorrhagic stroke is supportive treatment because no specific medication has been developed.[4,5] Therefore, treatments for acute ischemic and hemorrhagic stroke continue to be a major unmet clinical need.

We previously showed that miR-195 exerts vasculoprotective effects.[6] In addition, aberrant expression of miR-195 has been reported to play a role in neurological and cardiovascular diseases.[7–10] Stroke is a vascular disorder that leads to neural death. Because miR-195 plays roles in both the cerebrovascular and neural systems, dys-regulation of miR-195 levels may be associated with stroke event and prognosis. The primary aim of the present study is to test whether and how miR-195 is involved in stroke. To test our aim, we first investigated the mechanisms behind the of beneficial effects exhibited by miR-195 using endothelial cells, vascular smooth muscle cells, neural cells, and neural stem cells (NSCs). On the basis of the results of these cellular studies, we reasoned that miR-195 may be useful when applied to cerebrovascular events, regardless of ischemic or hemorrhagic stroke. Subsequently, we used miR-195 to treat animals with acute ischemic and hemorrhagic stroke. The results of these animal studies confirmed the potential role of miR-195 in stroke therapy.

RESULTS

miR-195 Exerts Neuroprotection

miR-195 Increases Viability of Damaged Cells

SH-SY5Y neural cells were subjected to oxygen-glucose deprivation (OGD) for 3 or 6 h to mimic ischemic conditions in the brain.

Received 27 November 2018; accepted 29 November 2018;
https://doi.org/10.1016/j.omtm.2018.11.011.

[10]These authors contributed equally to this work.

Correspondence: Suh-Hang H. Juo, Institute of New Drug Development, China Medical University, 91 Hsueh-Shih Road, Taichung 40402, Taiwan.
E-mail: hjuo@mail.cmu.edu.tw

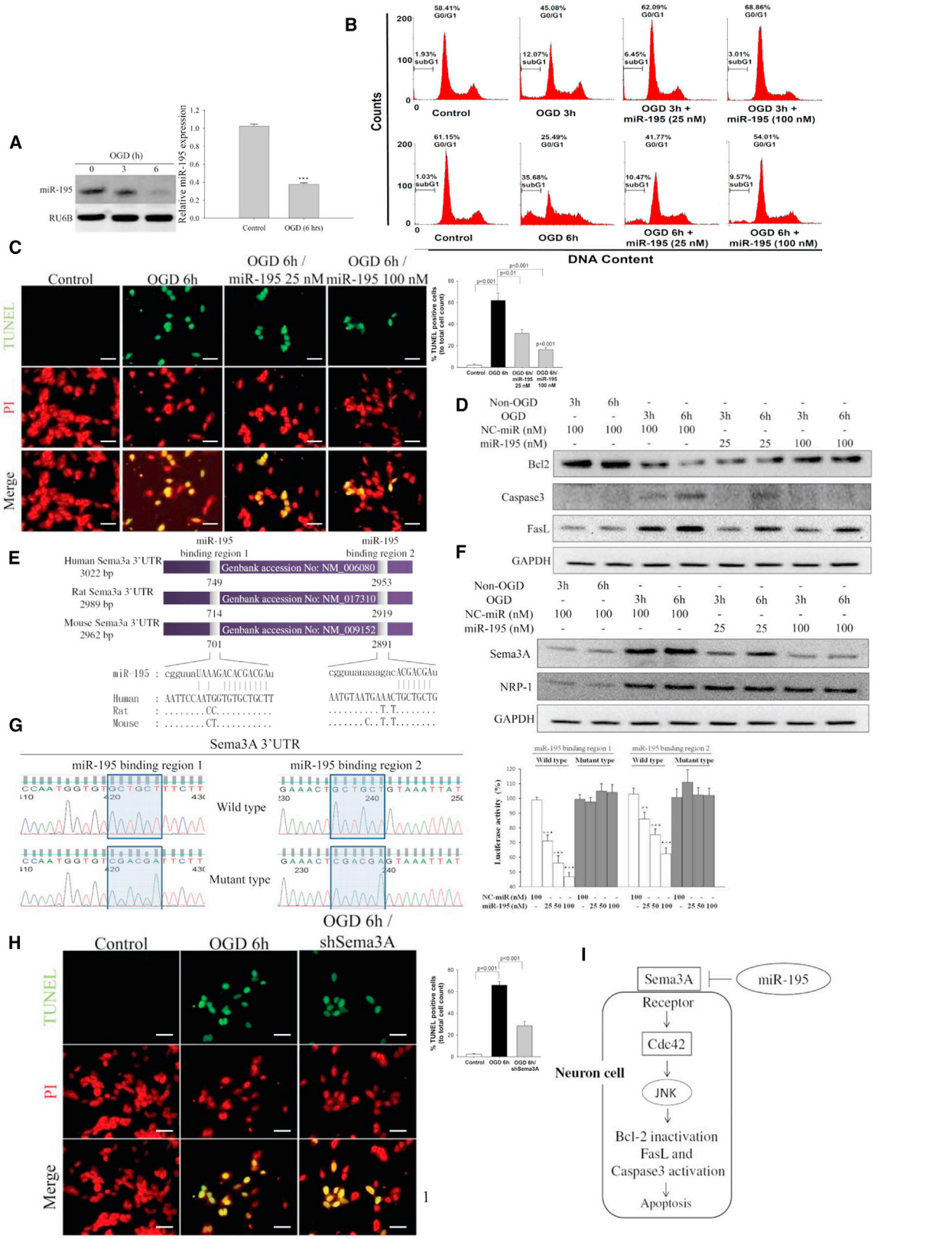

(legend on next page)

At 24 h, and miR-195 levels were significantly reduced (Figure 1A). In addition, OGD reduced cell viability and increased lactate dehydrogenase (LDH) release in a duration-dependent manner (Figures S1A and S1B). Transfection of miR-195 dose-dependently increased cell viability and decreased LDH release (Figures S1C and S1D). Flow cytometry analysis revealed that OGD increased SH-SY5Y cell entry into the sub-G1 phase, while miR-195 reduced the number of cells in the sub-G1 phase and restored the normal cell distribution in the G0/G1 phase (Figure 1B). TUNEL assay further demonstrated that miR-195 substantially decreased OGD-induced cellular apoptosis (Figure 1C). Besides, an increase in intracellular miR-195 levels led to upregulation of anti-apoptotic factor (Bcl-2) and downregulation of two apoptotic molecules (FasL and caspase-3) (Figure 1D). These results suggest that miR-195 possesses a neuroprotective effect by anti-apoptosis.

miR-195 Suppresses Sema3A Expression

Semaphorin 3A (Sema3A) is a potent inducer for neuronal death.[11,12] The Sema3A gene was predicted as a direct target of miR-195 by bioinformatic databases. There are two potential miR-195 binding sites at the *Sema3A* mRNA 3′ UTR in human, rat, and mouse (Figure 1E). We also experimentally confirmed that *Sema3A* can be knocked down by miR-195 (protein data in Figure 1F; RNA data in Figure S2). The luciferase reporter assay confirmed that miR-195 can bind to both binding sites in the Sema3A 3′ UTR (Figure 1G). The expression levels of Sema3A and its receptor, neuropilin (Nrp-1), were significantly increased in OGD-treated SH-SY5Y cells (protein data in Figure 1F; RNA data in Figure S2).

Knockdown of *Sema3A* reduced cell apoptosis (Figure 1H), increased cell count, and reduced LDH release (Figures S3A–S3C), confirming that miR-195's neuroprotective effect can be mediated through Sema3A repression. Cdc42 can affect cell cycle progression, regulate FasL expression,[13] activate caspase-3, and induce apoptosis.[14,15] We previously demonstrated that Cdc42 is also a direct target of miR-195[6]; furthermore, Cdc42 is a downstream molecule in the Sema3A signaling pathway.[16,17] Therefore, suppression of Sema3A also resulted in Cdc42 downregulation (Figure S3D). These data suggest that miR-195 can regulate *Sema3A* and *Cdc42* to achieve a neuroprotective effect. The miR195/Sema3A signaling pathway is schematically presented in Figure 1I.

miR-195 Improves Endothelial Functions

Given that endothelial cells (ECs) play multiple pivotal roles in stroke recovery, we tested the effects of miR-195 on endothelial functions. Transfection of miR-195 to human umbilical vein ECs (HUVECs) downregulated the expression of adhesion molecules and upregulated endothelial nitric oxide synthase (eNOS) expression (Figure 2A). To further mimic *in vivo* conditions, we assessed the effects of miR-195 on HUVECs in a HUVEC/human aortic smooth muscle cell (HASMC) co-culture. In the adhesion assay, oxidized low-density lipoprotein (oxLDL) treatment to HASMCs increased THP-1 adhesion to HUVECs in the HUVEC/HASMC co-culture. However, if oxLDL-treated HASMCs were also transfected with miR-195, THP-1 adhesion to HUVECs was reduced (Figure 2B).

miR-195 Inhibits NF-κB Signaling in ECs

NF-κB signaling affects the expression of adhesion and inflammatory molecules in ECs.[18,19] We conducted a series of experiments to show that miR-195 inhibits NF-κB signaling, including IKKα and phosphorylated IκBs (p-IκBα and p-IκBβ) (Figure 2A). These inhibitory effects subsequently reduced ubiquitin-dependent IκB degradation and led to suppression of p65/p50 (p65 is also known as RelA) and RelB/p52 nuclear transposition. (Figure S4).

CD40 is a protein expressed in the brain's neural and vascular cells that can stimulate the NF-κB pathway and was predicted to be a miR-195 direct target (Figure S5A).[20] CD40 expression is markedly upregulated in the stroke hemisphere, and its levels are related to post-ischemia brain inflammation.[20] Our experiments confirmed that CD40 was directly suppressed by miR-195 (Figures 2A and 5B). Knockdown of CD40 in HUVECs reduced cell adhesion (Figures 2C and 2D), decreased NF-κB signaling, and increased eNOS levels (Figure 2D).

miR-195 Stimulates Neural Stem Cells

Proliferation and mobilization of NSCs are important factors for stroke recovery.[21]

We used Nestin and SOX2 as NSC markers. Transfection of miR-195 to rat $Nestin^+/SOX2^+$ NSCs increased NSC proliferation (Figure 2E). SDF-1 can increase stem cell proliferation and promote NSC function. SDF-1 secretion was increased by transfection of miR-195 to

Figure 1. miR-195 Reversed OGD-Induced Apoptosis by Knockdown of Sema3A

All data presented in this figure were measured 24 h after the initiation of OGD. (A) Under 6 h OGD treatment, miR-195 levels were significantly decreased as measured by northern blot and qPCR. See also Figure S1. (B) Typical DNA histogram plots from flow cytometry of OGD-treated SH-SY5Y cells. miR-195 was transfected to the cells after 3 or 6 h of OGD. OGD increased the proportion of cells in sub-G1, and miR-195 reversed the cell distribution in the cell cycle. (C) TUNEL assay shows an increase of OGD-induced SH-S5Y5 apoptosis and miR-195 anti-apoptosis in a dose-dependent manner. Images were obtained using a Leica DMI6000B microscope with 400× magnification. Scale bar, 20 μm. (D) Transfection of miR-195 could reverse the detrimental effects of OGD by increasing an anti-apoptotic factor (Bcl-2) and suppressing apoptotic factors (FasL and caspase-3). (E) Schematic representation of miR-195 binding sites in the Sema3A 3′ UTR of human, rat, and mouse genome. (F) OGD treatment increased protein levels of Sema3A and its receptor Nrp-1, but miR-195 reversed the OGD effect on Sema3A. See RNA data in Figure S2. (G) The two miR-195 binding sites in the Sema3A 3′ UTR were individually tested using the luciferase reporter assay. miR-195 dose-dependently inhibited luciferase activity for the constructs carrying the wild-type sequence, but miR-195 had no effects on the constructs carrying the mutant sequence. (H) TUNEL assay demonstrates that Sema3-shRNA (short hairpin RNA) reduced apoptosis in the 6 h OGD-treated cells. See also Figures S3A–S3C. Images were obtained using a Leica DMI6000B microscope with 400× magnification. Scale bar, 20 μm. (I) Schematic diagram shows how miR-195 exerts its effect to prevent cell apoptosis. NC-miR, normal control microRNA; PI, propidium iodide stain. Lipofectamine 2000 was used for miR-195 transfection. $^{**}p < 0.01$ and $^{***}p < 0.001$. All values were expressed as mean ± SE.

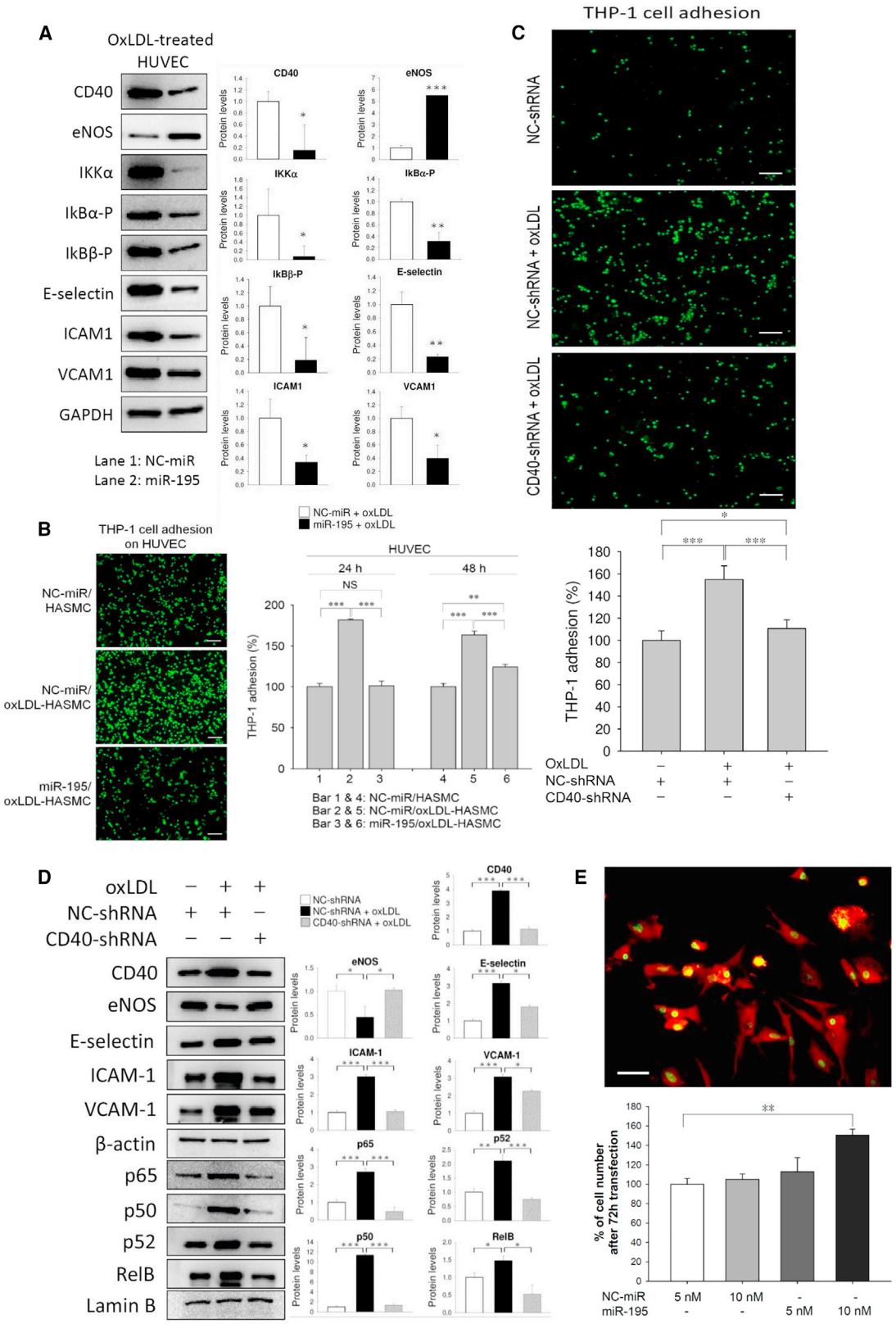

(legend on next page)

HASMCs (Figure S6A), but miR-195 did not have the same effect when transfected to HUVEC, mouse brain ECs, or astrocytes (Figures S6A–S6C).

Exogenous miR-195 Treats Acute Ischemic Stroke

Given that miR-195 has multiple beneficial effects on the neurovascular system, we tested whether miR-195 could be used to treat acute stroke. First, we induced ischemic stroke in rats by middle cerebral artery occlusion (MCAO).[22] We used two different types of MCAO: (1) permanent MCAO, in which the artery was occluded for 24 h and the rats were sacrificed directly thereafter, and (2) transient MCAO, in which the artery was occluded for 2 h and the rats were sacrificed on day 5. miR-195 carried by the commercial PEI-based nanoparticles (called *in vivo*-jetPEI) was IV injected via the tail vein. Our preliminary study found that the optimal concentration was 10 nmol/kg (Figure S7). For the rats subjected to permanent MCAO, miR-195 was injected at different time windows (0.5, 3, 4.5, and 6 h) after stroke. For the rats subjected to transient MCAO, miR-195 was given only at 6 h after stroke. NC-miR carried by *in vivo*-jetPEI was used as a placebo. To make the data comparable among rats subjected to transient MCAO, we calculated Garcia scores at 6 h post-stroke and selected only the rats with the scores between 6 and 8 for subsequent studies. As a result, all rats had similar levels of neurological deficiency upon enrollment for the study of transient MCAO.

The average infarct area of the treated group was significantly smaller than that of the placebo group for both permanent (Figures 3A and 3B) and transient (Figure 3C) MCAO models. More important, miR-195 retained its therapeutic effect at the intervention time window of 6 h. Significant improvements in Garcia score were noted on days 3 and 5 in the transient MCAO rats (Figure 3D). In the miR-195-treated rats, miR-195 levels were higher in the lesion cortex and subcortex than in the contralateral normal cortex and subcortex (Figure 3E). Conversely, in the placebo group, miR-195 levels were significantly lower in the lesion cortex and subcortex than in their counterparts. Furthermore, there was a negative correlation between miR-195 levels in the infarct hemisphere and infarct size (Pearson correlation = −0.78, $p = 0.0075$; Table S1).

Pharmacokinetics and Biodistribution

Seven normal Sprague-Dawley (SD) rats were independently used to test miR-195 concentrations in the circulation (i.e., pharmacokinetic study). Five minutes after injection of nanoparticle-carried miR-195 (10 nmol/kg), circulating miR-195 levels had increased by more than 390-fold (ranging from 390-fold to 1,025-fold). The half-life ($T_{1/2}$) varied among animals from a minimum of 893 min to a maximum of 6,650 min (Table S2). jetPEI can interfere with miR-195 detection. The wide range of $T_{1/2}$ may be because the dissociation of miR-195 from jetPEI varied among animals. Another 18 normal SD rats received the same treatment and were used to measure the distribution of miR-195 in the rats' organs. At each of the six time points (pre-dose and 1, 6, 24, 48, and 72 h), three rats were sacrificed. As expected, the highest concentration was in the serum, followed by the heart and then the lungs (Figure S8). Because these animals did not have stroke, the exogenous miR-195 barely affected miR-195 levels in the brain.

Confirmation of miR-195 Effects In Vivo

To replicate the effects of miR-195 demonstrated in our cellular studies, we measured anti-apoptotic markers, inflammatory substances, endothelial functions, and NSCs in the rodent brains subjected to permanent MCAO. The expression patterns of Sema3A, Nrp1, caspase-3, FasL, CdC42, and Bcl-2 in the brains were consistent with the results we obtained in the cellular studies (Figures 3F and 3G). Similarly, miR-195 possessed anti-inflammatory effects by decreasing TNFα, IL-1β, IL-6, and MCP-1 levels in the brains (Figure S9). Again, improvement of endothelial function by miR-195 was demonstrated through changes of the mRNA levels of inducible nitric oxide synthase (iNOS), eNOS, vascular cell adhesion molecule (VCAM), and intercellular adhesion molecule (ICAM) in the brains (Figure S10).

To demonstrate the effect of miR-195 on NSCs *in vivo*, we examined the brains from rats subjected to transient MCAO. On day 5 post-stroke, SDF-1 levels were higher in the miR-195-treated rats than in the NC-miR placebo rats (Figure 4A). Most NSCs co-expressed both SOX2 and Nestin markers. Both $SOX2^+/Nestin^+$ cells in the subventricular zone (SVZ) (Figure 4B) and peri-third ventricle (Figure 4C) were significantly increased in the miR-195-treated group compared with the placebo group. Notably, because stroke can also increases NSC proliferation, as a result there were more NSCs on the ischemic side (ipsilateral) than the uninjured contralateral side of the placebo group (Figure 4C). GAP43 is highly expressed in neuronal growth cones during development and axonal regeneration; therefore, the $GAP43^+$ cells indicated that miR-195 promoted

Figure 2. miR-195 Improved Endothelial Functions

(A) Protein markers in miR-195-transfected and oxLDL-treated HUVECs. We used oxLDL to decrease endothelial functions, and therefore the beneficial effects of miR-195 could be detected. Quantitative data from the western blot are shown at right. See also Figures S4 and S5. (B) HUVECs were co-cultured with microRNA-transfected (50 nmol/L) and oxLDL-treated HASMCs for 5 h, and the adhesion test was performed using THP-1 cells. Left: results obtained using a fluorescence microscope with 100× magnification; right: quantitative data. Scale bar, 100 μm. Lipofectamine 2000 was used as a transfection reagent. (C) HUVECs were transfected with CD40-shRNA (1 μg/mL), and THP-1 cells were added to the HUVEC culture for the adhesion assay at 5 h post-transfection. Images were obtained using a Leica DMI6000B microscope with 100× magnification. Scale bar, 100 μm. (D) Western blot for adhesion molecules, eNOS, and the NF-κB-related molecules was measured at 48 h post-transfection of shRNA. (E) Rat neural stem cells (NSCs) isolated from the subventricular zone (SVZ) were first confirmed by the positive staining of Nestin (red in cytoplasm) and Sox2 (green in nucleus and cytoplasm). Transfection of miR-195 by HiPerFect transfection reagent increased the proliferation of NSC at 72 h. Images were obtained using a Leica DMI6000B microscope with 400× magnification. Scale bar, 20 μm. Values are presented as mean ± SEM from three independent experiments performed in triplicate. *$p < 0.05$, **$p < 0.01$, and ***$p < 0.001$. NC-miR, normal control microRNA. All values were expressed as mean ± SE.

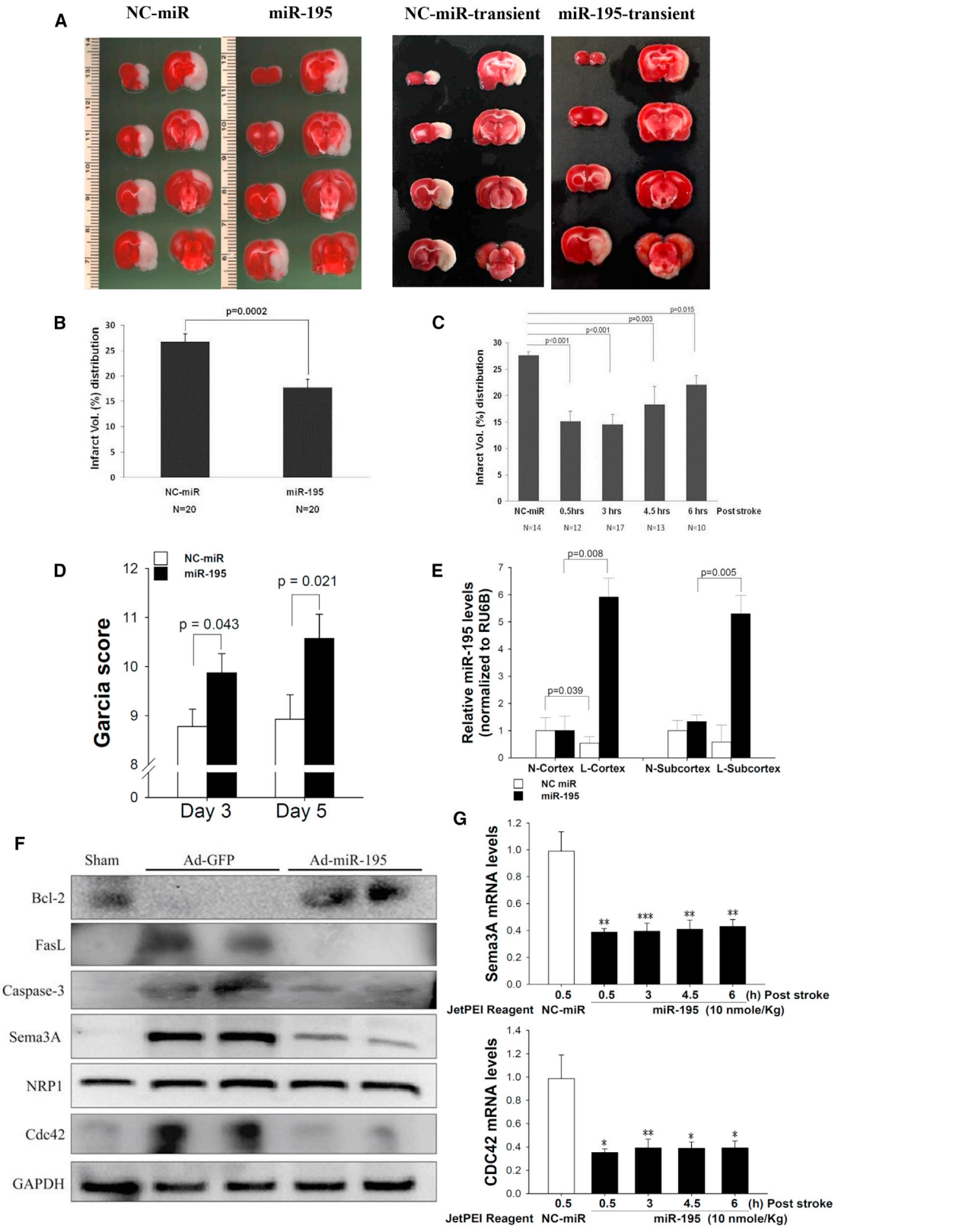

(legend on next page)

neuronal regeneration in multiple areas of the infarct brain (Figure 4D).

Exogenous miR-195 Treats Acute Hemorrhagic Stroke

We further examined the effect of miR-195 on acute hemorrhagic stroke in rats by IV injecting identically formulated miR-195 at 4 h post-stroke. The miR-195-treated group contained 31 rats, and the NC-miR placebo group contained 32 rats. All rats were evaluated for Garcia score, and the rats were sacrificed on day 3. Because the preparation of brain tissue for the measurement of edema, stroke lesion volume, and permeability differs, the rats were divided into groups of 16, 29, and 18 to be used for these three measurements, respectively. The results showed that miR-195 treatment significantly improved the functional outcome, as indicated by a higher Garcia score (all p values were 0.001 on days 1, 2, and 3; Figure 5A). miR-195 also significantly reduced brain edema ($p = 0.0006$; Figure 5B), lesion volume ($p = 0.01$; Figure 5C), and permeability ($p = 0.002$; Figure 5D) on day 3.

DISCUSSION

We showed that miR-195 can inhibit apoptosis in damaged neural cells, increase SDF-1 to promote NSCs for neurogenesis, block the NF-kB pathway for anti-inflammation, and improve endothelial functions. Figure 5E schematically shows the effects of miR-195 discovered in this study. These beneficial effects were also revealed by reduced brain damage and improved functional recovery in animals that had suffered from ischemic and hemorrhagic stroke. Accordingly, miR-195 possesses the potential to serve as a new drug to treat patients with acute stroke and other types of brain injury.

Current treatment and many ongoing clinical trials for ischemic stroke focus on thrombolytic therapy. However, it is important to distinguish whether the stroke is caused by ischemia or hemorrhage before using thrombolytic therapy, because this treatment may cause brain hemorrhaging that can further complicate the already injured brain. miR-195, on the other hand, has the potential to be used for both ischemic and hemorrhagic stroke; this advantage may make it more suitable for emerging treatment regardless of the stroke type. A recent breakthrough in treating acute ischemic stroke, intra-arterial clot retrieval, was validated in five clinical trials published in 2015.[23–27] Thus far, two strategies have been tested to treat ischemic stroke: restoring blood flow (tPA, clot retrieval) and reducing neural injury. These two strategies can have a synergistic effect. If miR-195 can be further proved effective in reducing brain injury, it may be applied to ischemic stroke patients before the procedure of clot retrieval is performed.

The change of miR-195 levels in damaged cells and tissues can be time, location, and cell type dependent. For example, the miR-195 level rapidly decreased in infarcted and border zones but dramatically increased in remote zones 1 h after myocardial ischemia.[28] On the contrary, prolonged myocardial ischemia caused the elevation of miR-195 levels in infarcted and border zones but suppression in remote zones.[28] Previous studies have reported that miR-195 can suppress anti-apoptosis gene BCL2 in cancer cell lines[29] and cardiomyoctes,[30] which opposes our finding in OGD-treated SY5Y cells. We also tested for the effect of miR-195 on mouse neural cell line (N2A cells) and found that miR-195 did not suppress BCL2 expression (Figure S11). Similar to our findings, Ai et al.[7] showed that miR-195 decreased in hypoxia-damaged neurons and reported that miR-195 prevented neuron death by suppressing the caspase pathway.[31] It should be noted that microRNA's suppressive effect is influenced by its target gene expression level, and a single microRNA can exert opposite effects under different conditions.[32,33] Therefore, the effects of miR-195 in different cells and organs may not be directly comparable.

Sema3A is upregulated when the brain is injured.[34] The increase in Sema3A signaling elevates cerebrovascular permeability,[35] and secreted Sema3A can additionally interact with its receptor Nrp-1 to inhibit neuronal regeneration and enhance neuronal death.[11,34,36] Sema3A can upregulate Cdc42 expression, and a decrease in Cdc42 expression has been reported to attenuate neuronal apoptosis in the rodent stroke model.[37] By inhibiting the cascade of Sema3A/Nrp-1/Cdc42 and increasing Bcl-2 levels, miR-195 can achieve an anti-apoptotic effect in the injured brain and reduce neuronal death. Consistent with our results, a recent study further demonstrated a significant decrease of infarct volume in Sema3A-knockout mice subjected to ischemic stroke.[35]

NSCs play a critical role in neurogenesis after stroke. NSCs need to migrate from the stem cell niches to the peri-infarct area to perform neurogenesis. We examined NSCs in the classic SVZ niche and a

Figure 3. miR-195 Improved Outcomes of Ischemic Stroke in Rats

Stroke rats were IV injected with miR-195 or NC-miR carried by jetPEI nanoparticles. The rodent brains subjected to permanent MCAO were collected at 24 h post-stroke, while brains of transient MCAO rodents were collected on day 5. (A) Representative brain slices from the permanent MCAO model (left panel) and the transient MCAO model (right panel). Rats subjected to permanent MCAO received NC-miR (left) or miR-195 (right) treatment at 3 h post-stroke, and they were sacrificed at 24 h. Rats subjected to transient MCAO received NC-miR or miR-195 treatment at 6 h post-stroke, and they were sacrificed on day 5. TTC staining (white) shows the infarct regions. (B) miR-195 significantly reduced the infarct volume in the permanent MCAO rats even when the treatment window was 6 h post-stroke. The infarct volumes are presented as a percentage of total brain volume. (C) miR-195 also significantly reduced the infarct volume in the transient MCAO rats treated at 6 h post-stroke. (D) miR-195 treatment improved the Garcia scores of the transient MCAO rats. N = 20 for each group. (E) miR-195 treatment of the permanent MCAO rats led to a high concentration of miR-195 in the stroke hemisphere. NC-miR treatment did not change miR-195 concentration in the lesion hemisphere. These rats received IV injection at 3 h post-stroke. L, stroke lesion hemisphere; N, normal hemisphere. N = 6 for NC-miR, n = 10 for miR-195. (F) Western blot for Sema3A, Nrp-1, Cdc42, Bcl-2, FasL, and caspase-3 in the brains of permanent MCAO rats treated with Ad-GFP or Ad-miR-195 at 3 h. GAPDH was used as the internal control. Ad-miR-195, adenovirus expressing miR-195; Ad-GFP, control adenovirus expressing GFP. (G) Brain sema3A and Cdc42 mRNA levels in the permanent MCAO rats treated with miR-195 or NC-miR at different time windows. N = 6, 10, 10, 10, and 8 for NC-miR and miR-195 at 0.5, 3, 4.5, and 6 h, respectively. *$p < 0.05$, **$p < 0.01$, and ***$p < 0.001$. All values were expressed as mean ± SE.

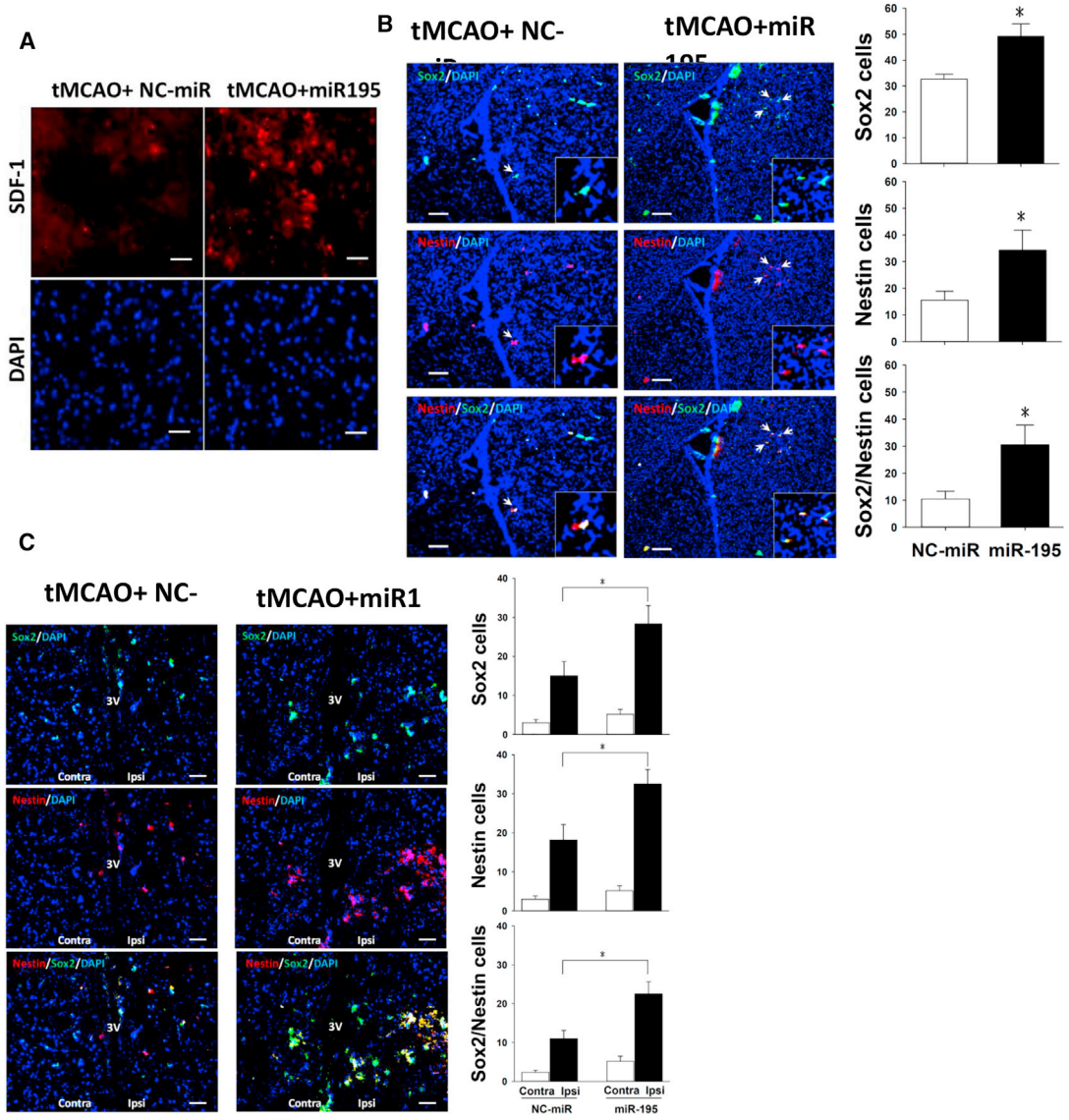

(legend on next page)

novel niche[38] (peri-third ventricle), and our data showed that miR-195 increased NSCs in both niches in the animals that had suffered strokes. These results were consistent with the previous report indicating that neurogenesis can be attributed to NSCs from multiple niches.[39] Numerous studies using the MCAO model have uniformly shown that proliferating NSCs are capable of migrating toward the injured sites in order to differentiate to new neurons.[38] However, NSCs can deplete over time after ischemic injury.[38] Our data revealed that miR-195 increases the number of NSCs and that these stem cells are likely to differentiate to functional neurons and glia because increased GAP43 expression was considered a marker of neuronal development and axonal regeneration.[40] Notably, GAP43 plays a role to regulate nerve sprout associated with adult plasticity.[41] Collectively, miR-195 may wake up stem cells from the niches and increase stem cell functions, leading to a better post-stroke outcome.

Stroke is more prevalent in the elderly, who often have chronic disease comorbidities. In this study, we induced artificial stroke in young animals. Therefore, the beneficial effects attributed to miR-195 may be attenuated in elderly subjects who suffer stroke. In the present study we did not measure physiological parameters for the stroke rats, and also we did not conduct longer term follow-up, which must be addressed in follow-up studies. Brain stroke triggers a complex and highly interconnected cascade of cellular and molecular events. Targeting multiple components of the neurovascular unit, rather than just neurons, should be a priority in stroke research.[42]

In conclusion, the present study not only demonstrated the detailed mechanisms of neurovascular protection controlled by miR-195 but also showed that miR-195 can be used to treat both acute ischemic and acute hemorrhagic stroke in experimental animals. Furthermore, the long time window for miR-195 treatment can be important for future clinical practice. Therefore, the potential of miR-195 to treat cerebral vascular accidents warrants further investigation.

MATERIALS AND METHODS

Detailed information can be found in the Supplemental Information.

Cell Studies

OGD was used to mimics ischemia *in vivo*. Cells were cultured in the OGD condition for 3 or 6 h, and then cells were maintained in glucose-containing DMEM with normoxia for 21 h (if OGD duration was 3 h) or 18 h (if OGD duration was 6 h). THP-1 cells were labeled with calcein AM and were added to the culture wells containing HUVECs for the monocyte adhesion assay. The luciferase reporter assay was used to test the existence of miR-195 binding sites in the targeted genes.

Target Site Prediction

Three algorithms were used to predict miR-195 target genes: miRanda (http://microrna.sanger.ac.uk/targets/v5/), TargetScan (http://targetscan.org), and PicTar (http://pictar.mdc-berlin.de).

Viral miR Preparation

Adenoviruses were amplified by infection into HEK293A cells. Viral MOI was estimated on the basis of *in vitro* HEK293A transduction efficiency: 0.5 mL of undiluted viral stocks were added to 10^6 HEK293A cells, and number of GFP-positive cells was counted 48 h after transduction.

Animal Study

The procedure for balloon injury[6] and for ischemic stroke by MCAO is described elsewhere.[22,43] In the present study's permanent MCAO model, male SD rats were subjected to occlusion for 24 h and sacrificed directly thereafter, because of the high mortality rate after 24 h MCAO. In the transient MCAO model, rats were subjected to occlusion for 2 h. In this model, rats were included for further evaluation only if their Garcia scores were between 6 and 8 at 6 h post-stroke. The eligible transient MCAO rats were then sacrificed on day 5. For hemorrhagic stroke, male SD rats were subjected to stereotaxic infusion of bacterial collagenase to induce intracranial hemorrhage (ICH). Similarly, we only included hemorrhagic stroke rats with moderate to severe neurological impairment, and these animals were sacrificed on day 3.

miR-195 mimic or normal control microRNA (NC-miR) was formulated with a commercial nanoparticle called jetPEI and then intravenously (IV) administrated via the tail vein. The operators were blinded to treatment assignment of miR-195 or NC-miR. The ischemic brain slices were stained with 0.1% 2,3,5-TTC. Digital photographs of the brain slices were taken, and lesion volume was computed using ImageJ version 1.40 (NIH). The total lesion volume was calculated as the sum of lesion area in each section.

The Garcia score was used to evaluate each rat's neurological function. The researchers who conducted the Garcia assessment were not informed of whether the rats were in the treated or placebo group. The assessment was performed on days 3 and 5 for transient MCAO rats and on days 1, 2, and 3 for hemorrhagic stroke rats. Because brain edema peaked on day 3 in hemorrhagic stroke, the brain was removed

Figure 4. miR-195 Promoted NSCs by Increasing SDF-1

(A) Stroke was induced by transient MCAO (tMCAO). miR-195 increased SDF-1 proteins in the cortex of stroke hemisphere, as indicated by immunofluorescent staining. Magnification, 200×. Scale bar, 20 μm. (B and C) miR-195 increased the number of $SOX2^+$ and $Nestin^+$ NSCs in the SVZ (B) and in the peri-third ventricle (3v) (C). NSCs were indicated by immunofluorescent staining. Insets show higher magnification for double-immunoreactive cells. *$p < 0.05$. Ipsi, the side ipsilateral to stroke lesion; Contra, the side contralateral to stroke lesion. Magnification, 100× for images in (B) and (C) and 400× for insets. Scale bar, 50 μm. The sample sizes for the bar charts in (B) and (C) were n = 6 for NC-miR and n = 6 for miR-195. (D) miR-195 increased the number of $GAP43^+$ cells (brown) indicated by immunohistochemistry staining in multiple areas of the stroke hemisphere. Magnification, 100×. Scale bar, 200 μm. tMCAO, transient middle carotid artery occlusion. Images were obtained using a Leica DMI6000B microscope. All values were expressed as mean ± SE.

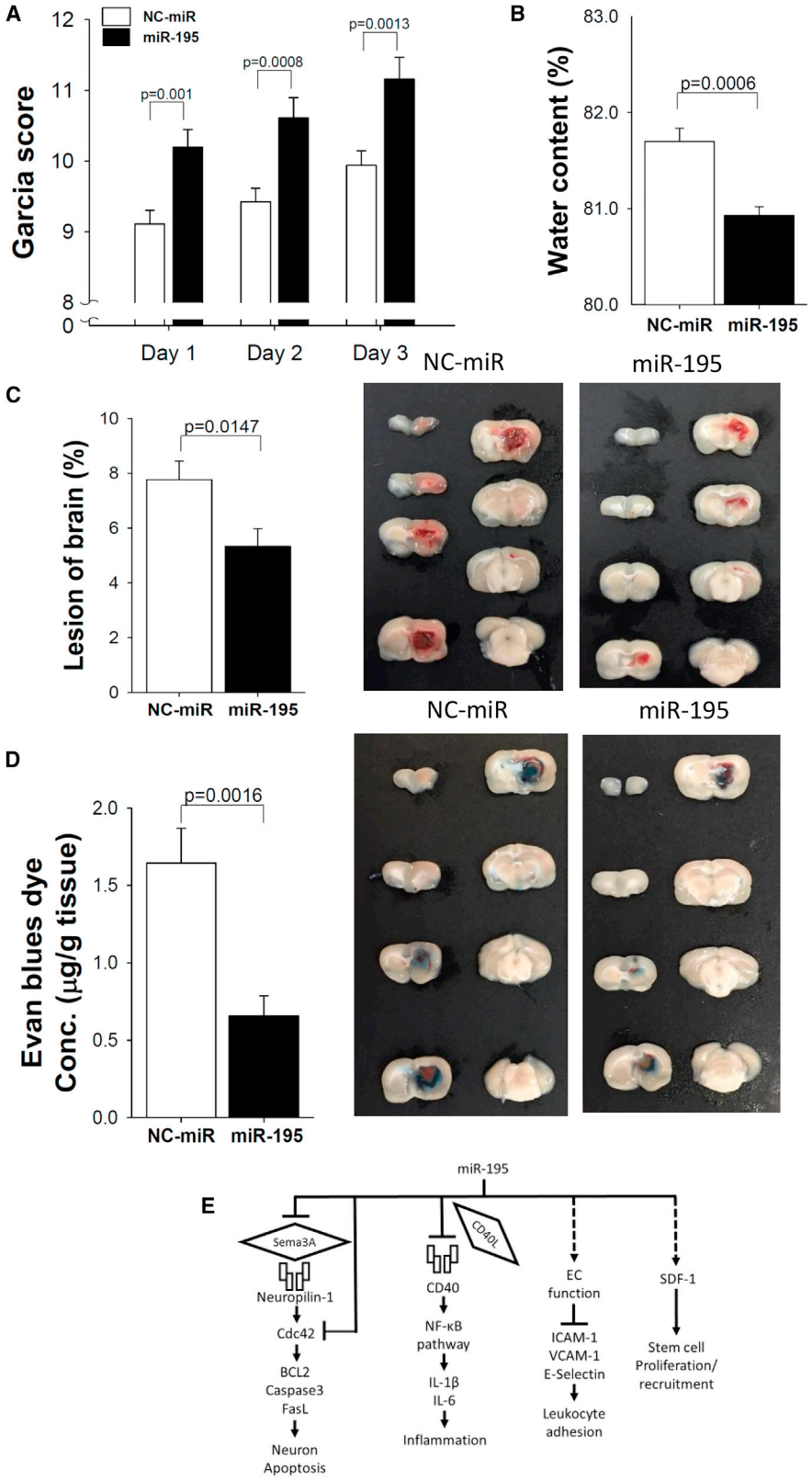

(legend on next page)

on day 3 and dried in an oven to obtain the dry weight. The cerebellum was used as an internal control. Water content was expressed as a percentage of wet weight: [(wet weight) − (dry weight)] (wet weight)$^{-1}$ × 100%. Blood-brain barrier permeability was assessed using a modified Evans blue extravasation method on day 3.

Immunostaining

Immunofluorescent staining was used to detect cellular expression of SDF-1, SOX2, Nestin, and GAP43. Immunohistochemistry (IHC) staining was used to stain the markers in brain slices.

Study Approval

The Animal Care and Use Committee of Kaohsiung Medical University approved the animal experimental protocols (approval number IACUC-101068), which strictly conforms to the NIH Guide for the Care and Use of Laboratory Animals (NIH Publication No. 85-23, revised 1996).

Statistical Analysis

All values in the text and figures are expressed as mean ± SE. Statistical differences were evaluated using Student's t test or analysis of covariance (ANCOVA). A p value less than 0.05 was considered to indicate statistical significance in all experiments. Analysis of the data and plotting of the figures were performed using SigmaPlot 10 software (Systat Software, San Jose, CA, USA).

SUPPLEMENTAL INFORMATION

Supplemental Information includes eleven figures, two tables, and Supplemental Materials and Methods and can be found with this article online at https://doi.org/10.1016/j.omtm.2018.11.011.

AUTHOR CONTRIBUTIONS

H.-Y.C. designed studies, conducted the experiments, interpreted the data, and wrote the draft. Y.-S.W. designed studies, conducted the experiments, interpreted the data, and wrote the draft. P.-Y.H. conducted the experiments and wrote the draft. C.-Y.C. conducted the experiments. Y.-C.L. designed studies, interpreted the data, and wrote the draft. S.-H.H.J. designed and supervised studies, interpreted the data, and wrote and proved the draft.

CONFLICTS OF INTEREST

H.-Y.C., Y.-S.W., and S.-H.H.J. have filed patents on the basis of the data from this study. The other authors have no competing interests. The authors have no additional financial interests.

ACKNOWLEDGMENTS

This work was supported by grants from the following organizations: the Department of Health (100TM014), the Ministry of Science and Technology (Taiwan, R.O.C., MOST103-2314-B-037-026-MY3, MOST 103-2314-B-037-027-MY2, MOST 105-2314-B-039-050, and MOST 106-2314-B-039-021), the National Health Research Institutes (Taiwan, R.O.C., NHRI-EX106-10605PI), Academia Sinica Taiwan Biobank Stroke Biosignature Project (BM10601010036), and "Drug Development Center, China Medical University" from The Featured Areas Research Center Program within the framework of the Higher Education Sprout Project by the Ministry of Education (MOE) in Taiwan.

REFERENCES

1. Feigin, V.L., Lawes, C.M., Bennett, D.A., Barker-Collo, S.L., and Parag, V. (2009). Worldwide stroke incidence and early case fatality reported in 56 population-based studies: a systematic review. Lancet Neurol. *8*, 355–369.
2. Cheng, N.T., and Kim, A.S. (2015). Intravenous thrombolysis for acute ischemic stroke within 3 hours versus between 3 and 4.5 hours of symptom onset. Neurohospitalist *5*, 101–109.
3. Reeves, M.J., Arora, S., Broderick, J.P., Frankel, M., Heinrich, J.P., Hickenbottom, S., Karp, H., LaBresh, K.A., Malarcher, A., Mensah, G., et al.; Paul Coverdell Prototype Registries Writing Group (2005). Acute stroke care in the US: results from 4 pilot prototypes of the Paul Coverdell National Acute Stroke Registry. Stroke *36*, 1232–1240.
4. Morgenstern, L.B., Hemphill, J.C., 3rd, Anderson, C., Becker, K., Broderick, J.P., Connolly, E.S., Jr., Greenberg, S.M., Huang, J.N., MacDonald, R.L., Messé, S.R., et al.; American Heart Association Stroke Council and Council on Cardiovascular Nursing (2010). Guidelines for the management of spontaneous intracerebral hemorrhage: a guideline for healthcare professionals from the American Heart Association/American Stroke Association. Stroke *41*, 2108–2129.
5. Steiner, T., Al-Shahi Salman, R., Beer, R., Christensen, H., Cordonnier, C., Csiba, L., Forsting, M., Harnof, S., Klijn, C.J., Krieger, D., et al.; European Stroke Organisation (2014). European Stroke Organisation (ESO) guidelines for the management of spontaneous intracerebral hemorrhage. Int. J. Stroke *9*, 840–855.
6. Wang, Y.S., Wang, H.Y., Liao, Y.C., Tsai, P.C., Chen, K.C., Cheng, H.Y., Lin, R.T., and Juo, S.H. (2012). MicroRNA-195 regulates vascular smooth muscle cell phenotype and prevents neointimal formation. Cardiovasc. Res. *95*, 517–526.
7. Ai, J., Sun, L.H., Che, H., Zhang, R., Zhang, T.Z., Wu, W.C., Su, X.L., Chen, X., Yang, G., Li, K., et al. (2013). MicroRNA-195 protects against dementia induced by chronic brain hypoperfusion via its anti-amyloidogenic effect in rats. J. Neurosci. *33*, 3989–4001.
8. Zhu, H.C., Wang, L.M., Wang, M., Song, B., Tan, S., Teng, J.F., and Duan, D.X. (2012). MicroRNA-195 downregulates Alzheimer's disease amyloid-β production by targeting BACE1. Brain Res. Bull. *88*, 596–601.
9. Sun, X.Y., Lu, J., Zhang, L., Song, H.T., Zhao, L., Fan, H.M., Zhong, A.F., Niu, W., Guo, Z.M., Dai, Y.H., et al. (2015). Aberrant microRNA expression in peripheral plasma and mononuclear cells as specific blood-based biomarkers in schizophrenia patients. J. Clin. Neurosci. *22*, 570–574.
10. Long, G., Wang, F., Duan, Q., Yang, S., Chen, F., Gong, W., Yang, X., Wang, Y., Chen, C., and Wang, D.W. (2012). Circulating miR-30a, miR-195 and let-7b associated with acute myocardial infarction. PLoS ONE *7*, e50926.
11. De Winter, F., Holtmaat, A.J., and Verhaagen, J. (2002). Neuropilin and class 3 semaphorins in nervous system regeneration. Adv. Exp. Med. Biol. *515*, 115–139.
12. Gagliardini, V., and Fankhauser, C. (1999). Semaphorin III can induce death in sensory neurons. Mol. Cell. Neurosci. *14*, 301–316.
13. Su, J.L., Lin, M.T., Hong, C.C., Chang, C.C., Shiah, S.G., Wu, C.W., Chen, S.T., Chau, Y.P., and Kuo, M.L. (2005). Resveratrol induces FasL-related apoptosis through

Figure 5. miR-195 Improved the Outcome of Hemorrhagic Stroke in Rats

(A) miR-195 treatment improved the Garcia score in the rats of hemorrhagic stroke; n = 32 for NC-miR, n = 31 for miR-195. (B) Reduced brain edema; n = 9 for NC-miR, n = 7 for miR-195. (C) Reduced percentage of lesion volume; n = 14 for NC-miR, n = 15 for miR-195. (D) Reduced blood-brain barrier (BBB) permeability; n = 9 for NC-miR, n = 9 for miR-195. (E) Schematic showing the effects of miR-195 on neurovascular protection. Values are presented as mean ± SEM from three independent experiments performed in triplicate. *p < 0.05, **p < 0.01, and ***p < 0.001. All values were expressed as mean ± SE.

Cdc42 activation of ASK1/JNK-dependent signaling pathway in human leukemia HL-60 cells. Carcinogenesis *26*, 1–10.

14. Manna, K., Khan, A., Kr Das, D., Bandhu Kesh, S., Das, U., Ghosh, S., Sharma Dey, R., Das Saha, K., Chakraborty, A., Chattopadhyay, S., et al. (2014). Protective effect of coconut water concentrate and its active component shikimic acid against hydroperoxide mediated oxidative stress through suppression of NF-κB and activation of Nrf2 pathway. J. Ethnopharmacol. *155*, 132–146.
15. Thomas, A., Giesler, T., and White, E. (2000). p53 mediates bcl-2 phosphorylation and apoptosis via activation of the Cdc42/JNK1 pathway. Oncogene *19*, 5259–5269.
16. Hou, S.T., Jiang, S.X., Desbois, A., Huang, D., Kelly, J., Tessier, L., Karchewski, L., and Kappler, J. (2006). Calpain-cleaved collapsin response mediator protein-3 induces neuronal death after glutamate toxicity and cerebral ischemia. J. Neurosci. *26*, 2241–2249.
17. O'Hare, M.J., Hou, S.T., Morris, E.J., Cregan, S.P., Xu, Q., Slack, R.S., and Park, D.S. (2000). Induction and modulation of cerebellar granule neuron death by E2F-1. J. Biol. Chem. *275*, 25358–25364.
18. Kouroedov, A., Eto, M., Joch, H., Volpe, M., Lüscher, T.F., and Cosentino, F. (2004). Selective inhibition of protein kinase Cbeta2 prevents acute effects of high glucose on vascular cell adhesion molecule-1 expression in human endothelial cells. Circulation *110*, 91–96.
19. Tzima, E., Del Pozo, M.A., Kiosses, W.B., Mohamed, S.A., Li, S., Chien, S., and Schwartz, M.A. (2002). Activation of Rac1 by shear stress in endothelial cells mediates both cytoskeletal reorganization and effects on gene expression. EMBO J. *21*, 6791–6800.
20. Klohs, J., Gräfe, M., Graf, K., Steinbrink, J., Dietrich, T., Stibenz, D., Bahmani, P., Kronenberg, G., Harms, C., Endres, M., et al. (2008). In vivo imaging of the inflammatory receptor CD40 after cerebral ischemia using a fluorescent antibody. Stroke *39*, 2845–2852.
21. Arvidsson, A., Collin, T., Kirik, D., Kokaia, Z., and Lindvall, O. (2002). Neuronal replacement from endogenous precursors in the adult brain after stroke. Nat. Med. *8*, 963–970.
22. Candelario-Jalil, E., Mhadu, N.H., González-Falcón, A., García-Cabrera, M., Muñoz, E., León, O.S., and Fiebich, B.L. (2005). Effects of the cyclooxygenase-2 inhibitor nimesulide on cerebral infarction and neurological deficits induced by permanent middle cerebral artery occlusion in the rat. J. Neuroinflammation *2*, 3.
23. Berkhemer, O.A., Fransen, P.S., Beumer, D., van den Berg, L.A., Lingsma, H.F., Yoo, A.J., Schonewille, W.J., Vos, J.A., Nederkoorn, P.J., Wermer, M.J., et al.; MR CLEAN Investigators (2015). A randomized trial of intraarterial treatment for acute ischemic stroke. N. Engl. J. Med. *372*, 11–20.
24. Goyal, M., Demchuk, A.M., Menon, B.K., Eesa, M., Rempel, J.L., Thornton, J., Roy, D., Jovin, T.G., Willinsky, R.A., Sapkota, B.L., et al.; ESCAPE Trial Investigators (2015). Randomized assessment of rapid endovascular treatment of ischemic stroke. N. Engl. J. Med. *372*, 1019–1030.
25. Campbell, B.C., Mitchell, P.J., Kleinig, T.J., Dewey, H.M., Churilov, L., Yassi, N., Yan, B., Dowling, R.J., Parsons, M.W., Oxley, T.J., et al.; EXTEND-IA Investigators (2015). Endovascular therapy for ischemic stroke with perfusion-imaging selection. N. Engl. J. Med. *372*, 1009–1018.
26. Saver, J.L., Goyal, M., Bonafe, A., Diener, H.C., Levy, E.I., Pereira, V.M., Albers, G.W., Cognard, C., Cohen, D.J., Hacke, W., et al.; SWIFT PRIME Investigators (2015). Stent-retriever thrombectomy after intravenous t-PA vs. t-PA alone in stroke. N. Engl. J. Med. *372*, 2285–2295.
27. Jovin, T.G., Chamorro, A., Cobo, E., de Miquel, M.A., Molina, C.A., Rovira, A., San Román, L., Serena, J., Abilleira, S., Ribó, M., et al.; REVASCAT Trial Investigators (2015). Thrombectomy within 8 hours after symptom onset in ischemic stroke. N. Engl. J. Med. *372*, 2296–2306.
28. Hang, P., Sun, C., Guo, J., Zhao, J., and Du, Z. (2016). BDNF-mediates down-regulation of microRNA-195 inhibits ischemic cardiac apoptosis in rats. Int. J. Biol. Sci. *12*, 979–989.
29. Singh, R., and Saini, N. (2012). Downregulation of BCL2 by miRNAs augments drug-induced apoptosis—a combined computational and experimental approach. J. Cell Sci. *125*, 1568–1578.
30. Zhu, H., Yang, Y., Wang, Y., Li, J., Schiller, P.W., and Peng, T. (2011). MicroRNA-195 promotes palmitate-induced apoptosis in cardiomyocytes by down-regulating Sirt1. Cardiovasc. Res. *92*, 75–84.
31. Chen, X., Jiang, X.M., Zhao, L.J., Sun, L.L., Yan, M.L., Tian, Y., Zhang, S., Duan, M.J., Zhao, H.M., Li, W.R., et al. (2017). MicroRNA-195 prevents dendritic degeneration and neuron death in rats following chronic brain hypoperfusion. Cell Death Dis. *8*, e2850.
32. Mukherji, S., Ebert, M.S., Zheng, G.X., Tsang, J.S., Sharp, P.A., and van Oudenaarden, A. (2011). MicroRNAs can generate thresholds in target gene expression. Nat. Genet. *43*, 854–859.
33. Shu, J., Xia, Z., Li, L., Liang, E.T., Slipek, N., Shen, D., Foo, J., Subramanian, S., and Steer, C.J. (2012). Dose-dependent differential mRNA target selection and regulation by let-7a-7f and miR-17-92 cluster microRNAs. RNA Biol. *9*, 1275–1287.
34. Jiang, S.X., Whitehead, S., Aylsworth, A., Slinn, J., Zurakowski, B., Chan, K., Li, J., and Hou, S.T. (2010). Neuropilin 1 directly interacts with Fer kinase to mediate semaphorin 3A-induced death of cortical neurons. J. Biol. Chem. *285*, 9908–9918.
35. Hou, S.T., Nilchi, L., Li, X., Gangaraju, S., Jiang, S.X., Aylsworth, A., Monette, R., and Slinn, J. (2015). Semaphorin3A elevates vascular permeability and contributes to cerebral ischemia-induced brain damage. Sci. Rep. *5*, 7890.
36. Pasterkamp, R.J., De Winter, F., Holtmaat, A.J., and Verhaagen, J. (1998). Evidence for a role of the chemorepellent semaphorin III and its receptor neuropilin-1 in the regeneration of primary olfactory axons. J. Neurosci. *18*, 9962–9976.
37. Zhao, J., Pei, D.S., Zhang, Q.G., and Zhang, G.Y. (2007). Down-regulation Cdc42 attenuates neuronal apoptosis through inhibiting MLK3/JNK3 cascade during ischemic reperfusion in rat hippocampus. Cell. Signal. *19*, 831–843.
38. Lin, R., and Iacovitti, L. (2015). Classic and novel stem cell niches in brain homeostasis and repair. Brain Res. *1628*, 327–342, Pt B.
39. Lin, R., Cai, J., Nathan, C., Wei, X., Schleidt, S., Rosenwasser, R., and Iacovitti, L. (2015). Neurogenesis is enhanced by stroke in multiple new stem cell niches along the ventricular system at sites of high BBB permeability. Neurobiol. Dis. *74*, 229–239.
40. Shen, Y., Mani, S., Donovan, S.L., Schwob, J.E., and Meiri, K.F. (2002). Growth-associated protein-43 is required for commissural axon guidance in the developing vertebrate nervous system. J. Neurosci. *22*, 239–247.
41. Frey, D., Laux, T., Xu, L., Schneider, C., and Caroni, P. (2000). Shared and unique roles of CAP23 and GAP43 in actin regulation, neurite outgrowth, and anatomical plasticity. J. Cell Biol. *149*, 1443–1454.
42. Candelario-Jalil, E. (2009). Injury and repair mechanisms in ischemic stroke: considerations for the development of novel neurotherapeutics. Curr. Opin. Investig. Drugs *10*, 644–654.
43. Wang, H.Y., Liu, C.B., Wu, H.W., and Kuo, J.S. (2010). Direct profiling of phospholipids and lysophospholipids in rat brain sections after ischemic stroke. Rapid Commun. Mass Spectrom. *24*, 2057–2064.

OMTM, Volume *13*

Supplemental Information

miR-195 Has a Potential to Treat Ischemic and Hemorrhagic Stroke through Neurovascular Protection and Neurogenesis

Hsin-Yun Cheng, Yung-Song Wang, Po-Yuan Hsu, Chien-Yuan Chen, Yi-Chu Liao, and Suh-Hang H. Juo

Supplemental Figures

(Suppl Fig1 A)

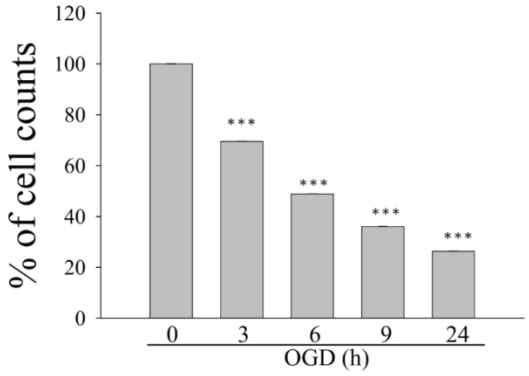

(Suppl Fig 1B)

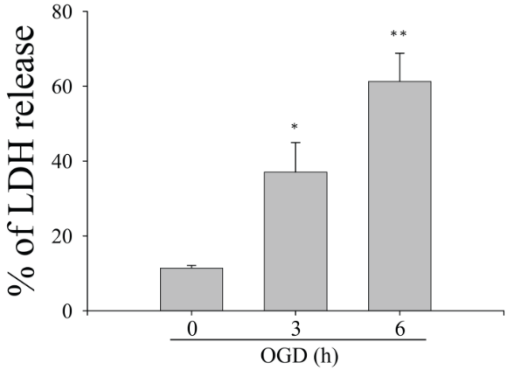

(Suppl Fig 1C)

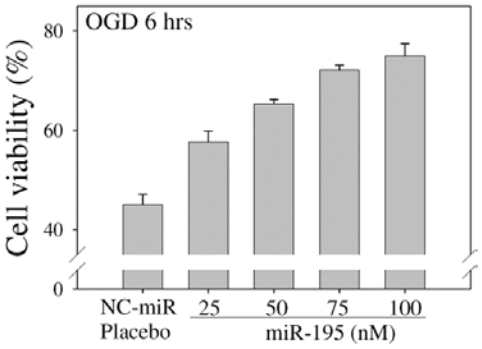

(Suppl Fig 1D)

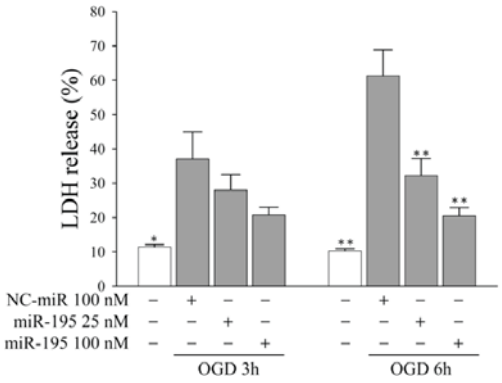

(Suppl Fig 2)

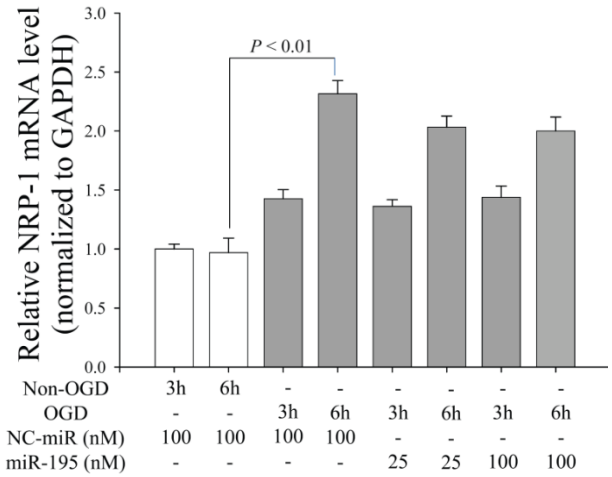
Relative NRP-1 mRNA level (normalized to GAPDH)
P < 0.01
3.0
2.5
2.0
1.5
1.0
0.5
0.0
Non-OGD 3h 6h - - - - - -
OGD - - 3h 6h 3h 6h 3h 6h
NC-miR (nM) 100 100 100 100 - - - -
miR-195 (nM) - - - - 25 25 100 100

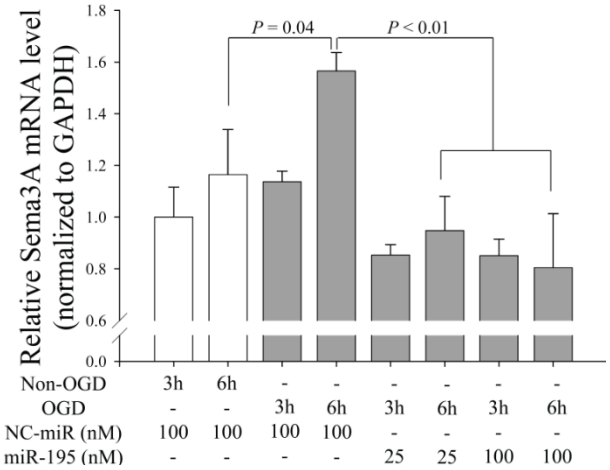
Relative Sema3A mRNA level (normalized to GAPDH)
P = 0.04
P < 0.01
1.8
1.6
1.4
1.2
1.0
0.8
0.6
0.0
Non-OGD 3h 6h - - - - - -
OGD - - 3h 6h 3h 6h 3h 6h
NC-miR (nM) 100 100 100 100 - - - -
miR-195 (nM) - - - - 25 25 100 100

(Suppl Fig 3A)

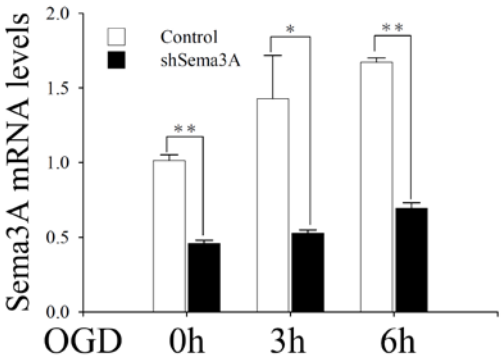

(Suppl Fig 3B)

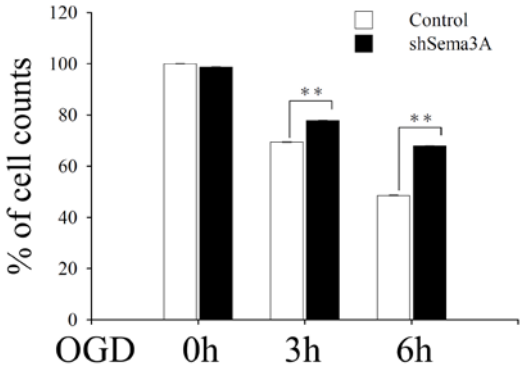

(Suppl Fig 3C)

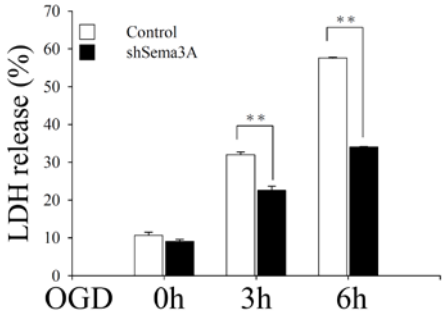

(Suppl Fig 3D)

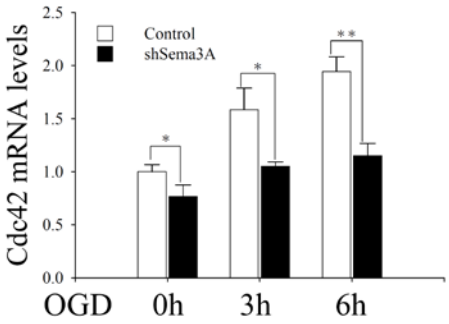

(Suppl Fig 4)

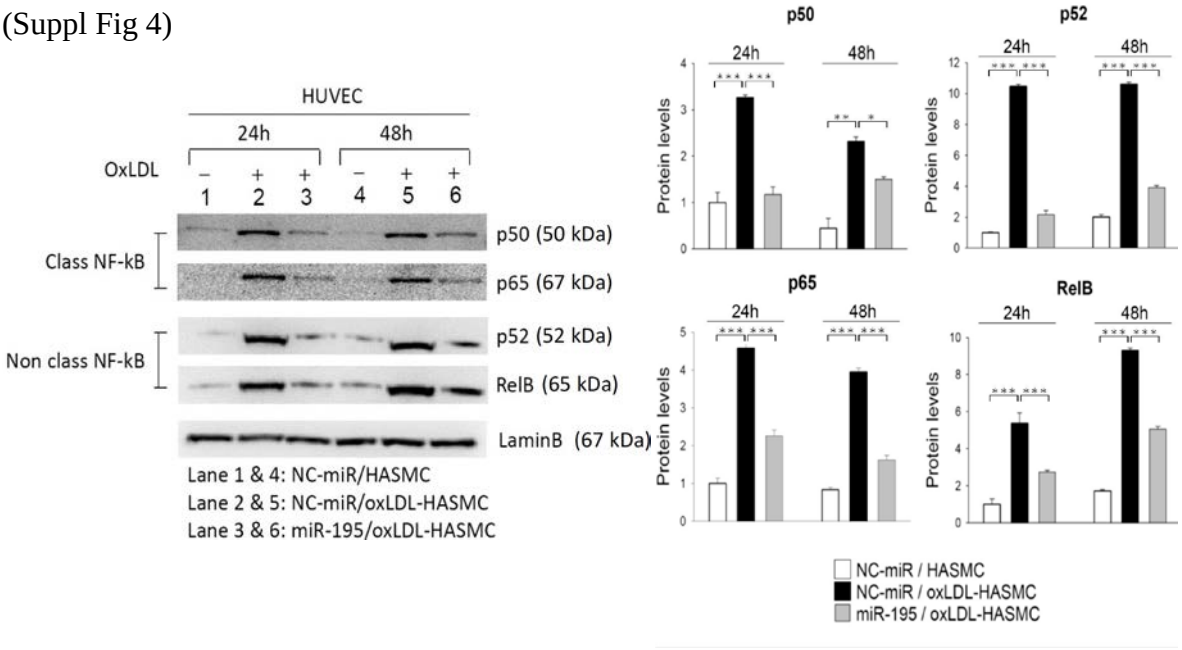
HUVEC
24h
48h
OxLDL
– + + – + +
1 2 3 4 5 6
Class NF-kB
Non class NF-kB
p50 (50 kDa)
p65 (67 kDa)
p52 (52 kDa)
RelB (65 kDa)
LaminB (67 kDa)
Lane 1 & 4: NC-miR/HASMC
Lane 2 & 5: NC-miR/oxLDL-HASMC
Lane 3 & 6: miR-195/oxLDL-HASMC
p50
p52
p65
RelB
24h
48h
Protein levels
NC-miR / HASMC
NC-miR / oxLDL-HASMC
miR-195 / oxLDL-HASMC

(Suppl Fig 5A)

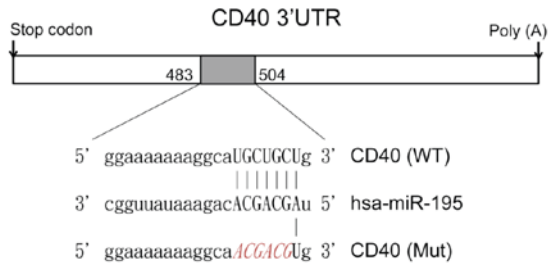

(Suppl Fig 5B)

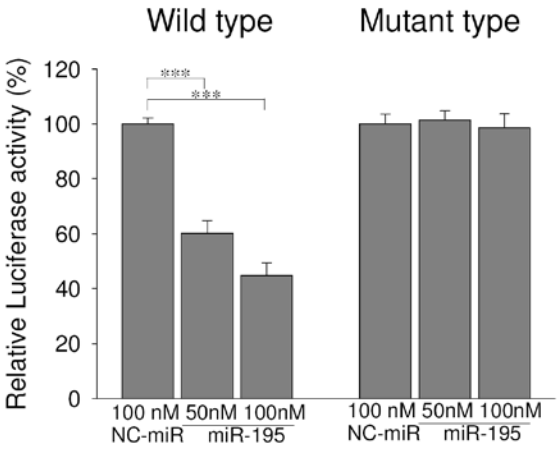

(Suppl Fig 6A)

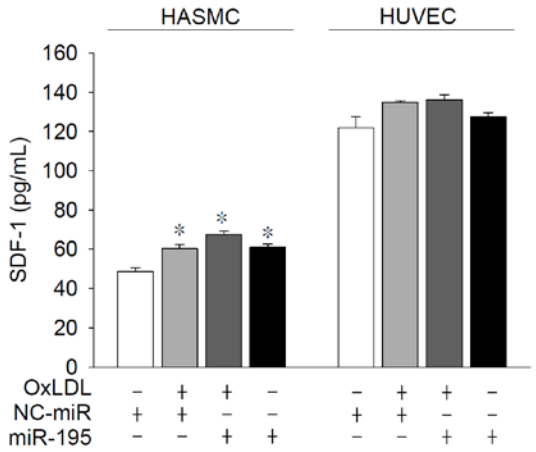

(Suppl Fig 6B)

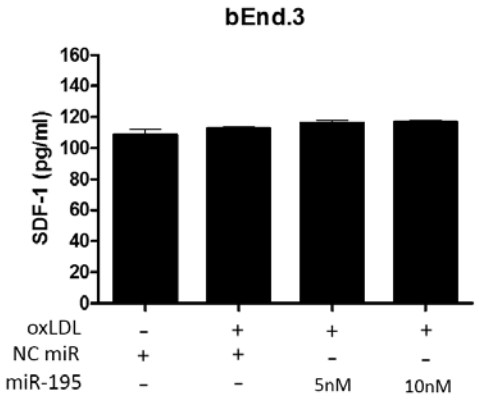

(Suppl Fig 6C, ALT cells)

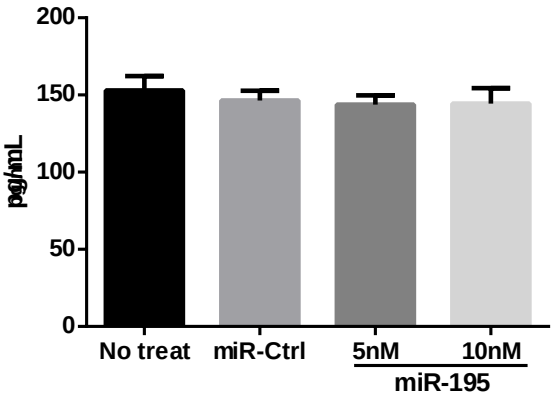

(Suppl Fig 7)

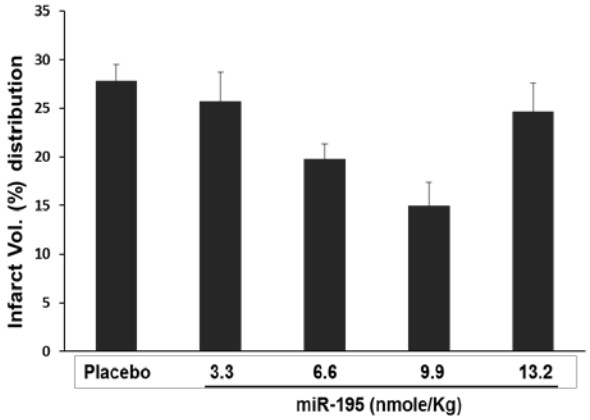

(Suppl Fig 8)

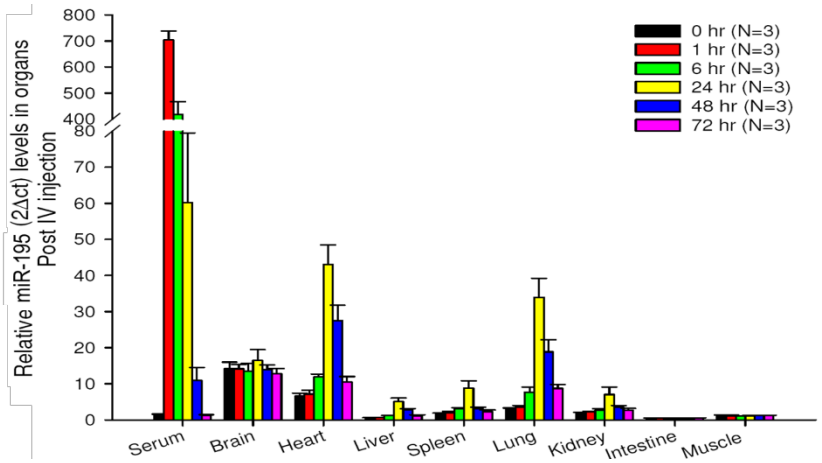

(Suppl Fig 9)

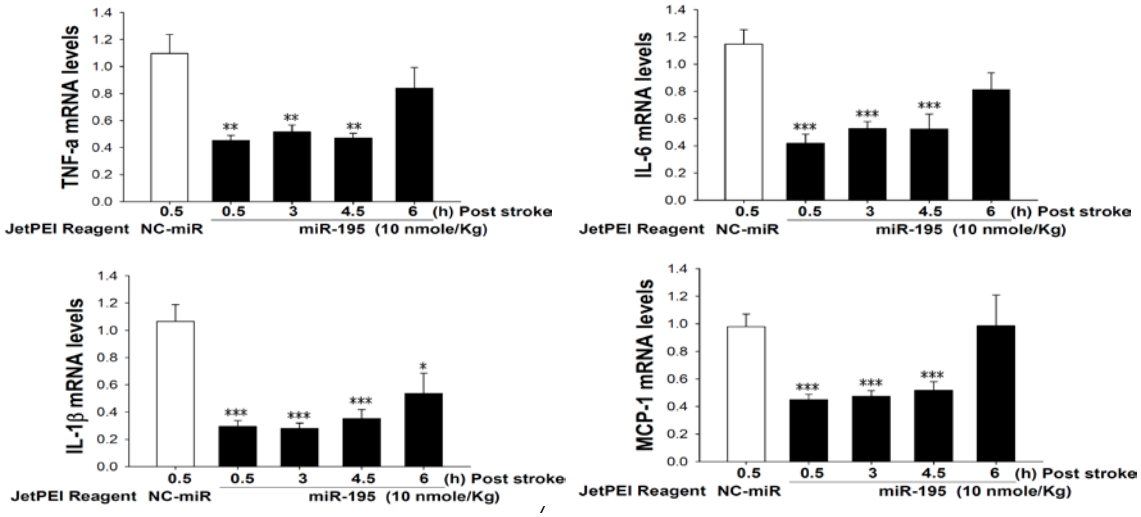

(Suppl Fig 10)

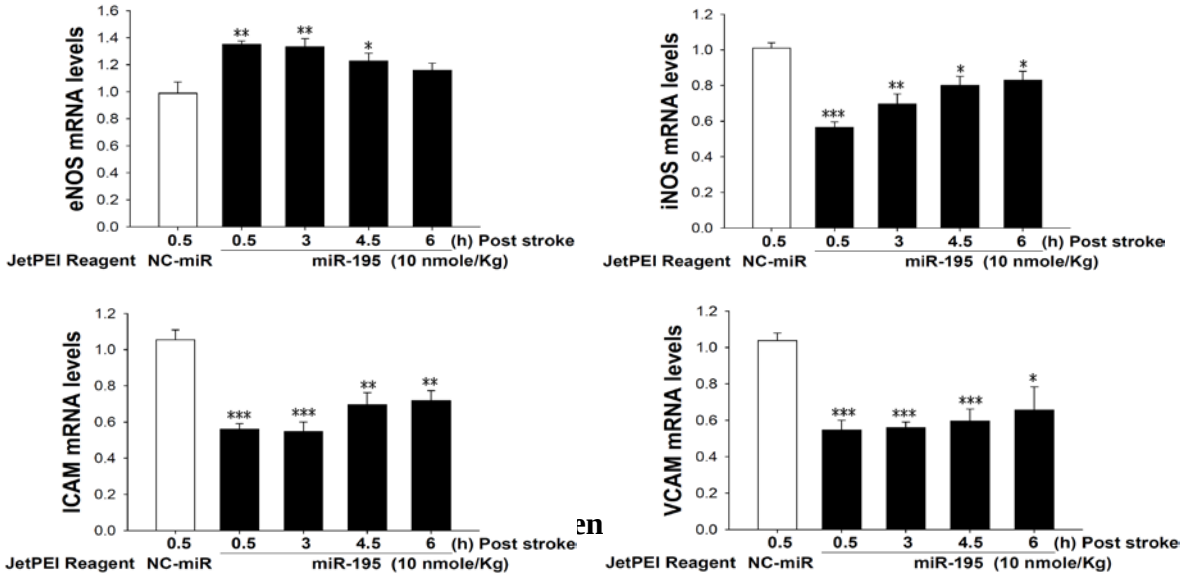

(Suppl Fig 11)

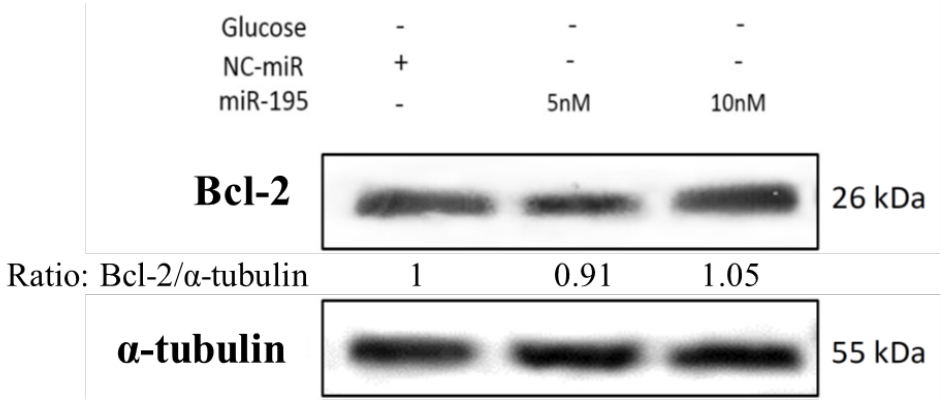

Supplemental Figure Legends

Supplemental. Fig 1. MiR-195 increased survival in OGD-treated SH-SY5Y cells

(A-D) The OGD treatment to SH-SY5Y cells induced a duration-dependent decrease of cell counts and an increase of LDH (A and B), which could be reversed by transfection of miR-195 (C and D). NC-miR: negative control microRNA. Data are means ± SE from three independent experiments performed in triplicates. *P<0.05, **P<0.01 and ***P<0.001 vs. control cells not exposed to OGD.

Supplemental Fig 2. miR-195 knocked down Sema3A mRNA level but had no effect on Nrp-1 mRNA level

Supplemental Fig 3. Knockdown of Sema3A eliminated the OGD effects.

(A) Sema3A level was increased by OGD in a duration-dependent manner and Sema3A-shRNA significantly suppressed OGD-induced Sema3A mRNA level.

(B-D) Sema3-shRNA eliminated the OGD effects on cell viability, LDH release and Cdc42 gene expression. Data are means ± SEM from three independent experiments performed in triplicates. *P<0.05 and **P<0.01 vs. control cells not exposed to OGD. Scrambled shRNA was used as transfection control.

Supplemental Fig 4. miR-195 inhibited nuclear translocation of NF-κB transcription complex

miR-195 influenced the nuclear translocation of NF-κB transcription complex in HUVECs when co-cultured with HASMCs. Nuclear extracts from HUVECs were analyzed by the western blot to detect p50, p65 (also known as RelA), p52 and RelB proteins. Lamin B was used as a nuclear marker. The Western blot data are shown in the left and the quantitative data in the right. Values are presented as mean ± SEM from 3 independent experiments performed in triplicates.

Supplemental Fig 5. miR-195 targeted and suppressed CD40 expression

(A) Sequence pairing revealed a miR-195 target site in the 3' UTR of the CD40 transcript. **(B)** the luciferase reporter assay showed a dose-dependent knockdown of luciferase activity by miR-195 which confirmed the miR-195 binding site in the CD40 3'UTR. miR-195 was transfected by using lipofetamine2000.

Supplemental Fig 6. miR-195 increased SDF-1 secretion

(A) Both miR-195 and oxLDL increased the SDF-1 release in the HASMC culture medium but not in HUVEC culture medium. **(B and C)** miR-195 did not increase SDF-1 release in the culture medium in the mouse brain endothelial cell line

(bEND.3) or in mouse astrocyte cell line (ALT cells). SDF-1 protein levels in culture medium were measured by ELISA. Data are presented as mean ± SEM from at least three independent experiments. **p<0.01, ***p<0.001

Supplemental Fig 7. miR-195 dose-response data

We conducted a dose escalation study to find the optimal dose of miR-195 (carried by jetPEI nanoparticles) in rats of permanent MCAO. The placebo was NC-miR carried by jetPEI nanoparticles. The sample sizes for placebo, 3.3, 6.6, 9.9 and 13.2 miR-195 (nmole/kg) were 3, 3, 9, 10 and 4, respectively. Based on this dose-ranging study, we decided to use 10 nmole/kg for the main animal study.

Supplemental Fig 8. miR-195 biodistribution

miR-195 carried by jetPEI nanoparticles was IV injected (10 nmole/kg) to 18 normal SD rats. miR-195 was detected by real-time PCR. Three rats were sacrificed at the following time points: pre-dose, 1h, 6h, 24h, 48h and 72h.

Supplemental Fig 9. miR-195 had anti-inflammatory effects in stroke animals.

The rats subjected to permanent MCAO were IV injected with miR-195 or NC-miR carried by jetPEI nanoparticles, and the brains were collected at 24hr post-stroke. miR-195 decreased TNFα, IL-1β, IL-6 and MCP-1 mRNA levels in the brains. The

sample size for NC-miR was 6. For miR-195 treatment at the time point of 0.3h, 3h, 4.5h and 6h, the sample size was 10, 10, 10 and 8, respectively. RNA data are presented as mean ± SE from qPCR performed in triplicates. *P< 0.05; **p<0.01; ***p<0.001.

Supplemental Fig 10. miR-195 exerted endothelial protection in stroke animals. The rats subjected to permanent MCAO were IV injected with miR-195 or NC-miR carried by jetPEI nanoparticles, and the brains were collected at 24hr post-stroke. miR-195 improved endothelial functions by altering mRNA levels of iNOS, eNOS, VCAM and ICAM. The sample size for NC-miR was 6. For miR-195 treatment at the time point of 0.3h, 3h, 4.5h and 6h, the sample size was 10, 10, 10 and 8, respectively. RNA data are presented as mean ± SE from qPCR performed in triplicates. *P< 0.05; **p<0.01; ***p<0.001.

Supplemental Fig 11. The effect of miR-195 effect on BCL2 expression in mouse neural cells (N2A)

Supplemental Table1. Negative correlation between miR-195 in the infarct hemisphere and infarct size.

	infarct size %	brain miR-195*	sema3A*
PEI195-D3H-1	3	4.52x	1.07x
PEI195-D3H-2	4.38	3.48x	0.9x
PEI195-D3H-3	5.02	2.97x	1.37x
PEI195-D3H-4	12.2	3.74x	1.16x
PEI195-D3H-5	12.62	2.05x	0.84x
PEI195-D3H-6	16.69	4.08x	0.96x
PEI195-D3H-7	21.49	2.34x	1.76x
PEI195-D3H-8	22.95	1.73x	3.44x
PEI195-D3H-9	24.56	1.85x	1.61x
PEI195-D3H-10	25.42	1.82x	1.54x

Spearman r=-0.78 (p=0.0075) between infract size and fold increase of miR-195.
*the ratio = RNA expression level in the infarct hemisphere/contralateral hemisphere

Supplemental Table 2. The calculate pharmacokinetics parameters.

The injected dose of 10 nmole/kg is equivalent to 6×10^{15} miR-195 copy/kg. Seven rats were used for this pharmacokinetic study. The first blood sample after miR-195 injection was withdrawn at 5 min.

λ_z: the elimination (terminal) rate constant.

$T_{1/2}$: the elimination (terminal) half-life.

T_{max}: the time at which C_{max} is reached.

C_{max}: the observed maximum (peak) plasma miR-195 concentration after dosing.

$AUC_{0\text{-}last}$: the area under the plasma miR-195 concentration-time curve from the time zero to that of the last sample assayed.

$AUC_{0\text{-}\infty}$: the area under the plasma miR-195 concentration-time curve from the time zero to infinity.

CL: the plasma clearance of the miR-195 from the body.

$MRT_{0\text{-}\infty}$: the mean residence time (MRT_0) extrapolated to infinity.

V_β: the volume of distribution at the elimination phase.

V_{ss}: the volume of distribution at steady-state.

Non-compartmental pharmacokinetic parameters are calculated using the WinNonlin™. The apparent plasma terminal elimination half-life ($T_{1/2}$) is calculated according to the following formula:

$$T_{1/2} = \ln(2)/ \lambda_z$$

The observed maximum plasma concentration (C_{max}) and the time of C_{max} (T_{max}) were determined directly from the experimental values. The area under the plasma concentration-time curve of miR-195 from time 0 to the last measurable concentration ($AUC_{0\text{-}last}$) was determined by the linear trapezoidal rule. The area under the plasma concentration-time curve from time 0 to infinity ($AUC_{0\text{-}\infty}$) was determined by $AUC_{0\text{-}last} + C_{last}/\lambda_z$.

Rat	λ_z (1/min)	$T_{1/2}$ (min)	T_{max} (min)	C_{max} (copy/mL)	$AUC_{0\text{-last}}$ (min*copy/mL)	$AUC_{0\text{-}\infty}$ (min*copy/mL)	CL (copy/ (min*copy/mL)/kg)	$MRT_{0\text{-}\infty}$ (min)	V_β (copy/ (copy/mL)/kg)	V_{ss} (copy/ (copy/mL)/kg)
1	0.000776	893.2743	5	3.43694E+13	1.97099E+15	1.97099E+15	2.930183	770.624	3776.192	2258.069
2	0.000435	1593.003	5	2.37986E+13	7.54123E+14	7.54123E+14	7.39451	1033.225	16994.19	7640.189
3	0.000426	1625.835	5	1.88531E+13	9.96471E+14	9.96471E+14	5.572238	1285.021	13070.15	7160.446
4	0.000405	1712.684	5	1.74402E+13	1.05939E+15	1.05939E+15	4.942568	1648.827	12212.49	8149.441
5	0.000647	1071.015	5	3.77593E+13	1.95273E+15	1.95273E+15	3.005403	556.7267	4643.792	1673.188
6	0.000104	6650.806	5	2.51089E+13	1.09389E+15	1.09389E+15	3.319097	6016.793	31847.02	19970.32
7	0.000293	2366.807	5	3.22587E+13	1.15722E+15	1.15722E+15	4.664472	1441.843	15927.22	6725.435

Supplemental Methods and Materials

Cell culture

Human neuroblastoma SH-SY5Y cells, Human THP-1 monocytic leukemia cells, human umbilical venous endothelial cells (HUVEC) were from American Type Culture Collection (ATCC). Mouse neuroblastoma cell line N2A cells and mouse brain endothelial cell line bEnd.3 cells were from Bioresource Collection and Research Center (Taiwan). The rat neural stem cells were isolated from SVZ. The components of culture medium for SH-SY5Y contain a 1:1 mixture of DMEM and Ham's F-12 medium, 10% heat-inactivated FBS, 4mM glutamine, 100 U/ml penicillin, 100 mg/ml streptomycin and 0.25 mg/ml amphotericin B at 37^{o}C in a humidified incubator under 5% CO_2 and 95% air. The medium was changed every 3-4 days. Cells were seeded in 96-well culture plates to measure cell viability at a density 1×10^5 cells/ml. N2A cells and bEnd.3 cells were maintained in DMEM supplemented with 10% FBS plus 50 μg/ml gentamicin in a humidified incubator under an atmosphere of 5% CO2/95% air at 37 °C.

Cell co-culture

For HASMC/HUVEC non-contact co-culture, HUVECs were seeded onto the 24-well plate at a density of 3×10^5 cells/cm^2. HASMCs were seeded on the filters of transwell insert (0.4 μm pore membrane; Millipore) at a density of 1×10^5 cells/cm^2. The insert was put on the top of 24-well plate as the co-culture system with or without the presence of oxLDL (40 μg/ml).

Oxygen–glucose deprivation and transfection of miRNA

The oxygen–glucose deprivation (OGD) condition mimics the in vivo ischemic condition. For OGD, SH-SY5Y cells were cultured with glucose-free DMEM (Gibco Inc.) and placed in the hypoxic chamber (5% CO_2, 1% O_2 and 94% N_2) for 3h or 6h. After OGD, SH-SY5Y cells were maintained in glucose-containing DMEM with normoxia (5% CO_2, 95% O_2) for 21h (if OGD duration was 3h) or 18h (if OGD duration was 6h). Control SH-SY5Y cells were cultured in the normoxic condition for 24 hrs. Cellular phenotypes and biomarkers were measured at 24^{th} hour after the initiation of OGD treatment.

Cell viability

The cell viability was determined by cell counts and lactate dehydrogenase (LDH) assay. Cells were seeded at a density of 1.5×10^5 cells per well on collagen coated 12-well plates and maintained at 37°C in a 5% CO2 atmosphere. After OGD and reoxygenation, an aliquots of cells were counted and stained with trypan blue to determine viability. Cell lysis was quantified after 4h of treatment with the test agents by LDH activity using the Cytotoxicity Detection KitPlus (Roche Applied Science, Germany). The plates were centrifuged at 400 g and 4^oC for 4 min and an aliquot of 50 µl was taken to quantify the LDH amount.

Cell cycle Analysis

OGD-induced SH-SY5Y cell death was identified as a sub-G1 peak in the cell cycle. Briefly, 5 x 10^6 harvested cells were washed in ice-cold PBS, fixed in ice-cold 70% ethanol and stored at 4^{o}C. Cells were then washed with PBS, treated with 0.5 mg/mL RNase (Sigma) at 37^{o}C for 15 min and finally stained with propidium iodide (Sigma, 50 μg/mL) in PBS. Cells were analyzed on a Coulter EPICS XL flow cytometer (System II software; Becton-Dickinson, CA, USA) and data were analyzed with Modifit LT 2.0 (Becton-Dickinson, CA, USA). 10,000 cells were counted for each determination. For detailed analysis, the three cell cycle compartments (sub-G1, G0/G1, S, and G2/M phases) were distinguished and the percentage of cells was quantified with CELLQuest software (Becton-Dickinson, CA, USA).

Detection of DNA fragmentation by TUNEL assay

For the TUNEL assay, the ApoAlert DNA fragmentation assay kit (Clontech, CA, USA) was used. The incorporation of fluorescein-dUTP into the fragmented nuclear DNA generates the green fluorescence detected by a standard fluorescein filter set (520 ± 20 nm). All cells stained with propidium iodide exhibited strong red cytoplasmic fluorescence when viewed at > 620 nm.

Luciferase reporter construct and assay

The plasmid construct was created to carry the predictive miR-195 binding site. A DNA segment containing miR-195 binding site in the wild-type 3'UTR was cloned into the Mlu I/Hind III site of the pMIR-REPORT Luciferase vector (Life Technologies). The mutant 3'UTR to destruct the miR-195 binding site was generated by site-directed mutagenesis as described previously (Brons-Poulsen et al., 1998). Plasmid constructs (carrying either wild or mutant type 3'UTR) and miR-195 were co-transfected into the HEK293A cells, and firefly and Renilla luciferase activity were measured at 24h using the Dual-Luciferase Reporter Assay. Each transfection was repeated twice in triplicate.

Target site prediction

Three algorithms were used to predict miR-195 target genes. The algorithms are miRanda algorithm (http://microrna.sanger.ac.uk/targets/v5/), TargetScan (http://targetscan.org/), and PicTar (http://pictar.mdc-berlin.de/). The binding sites of POU2F1 in the promoter region of COMP and Ang1 were predicted by the TFSEARCH promoter program (http:// www.cbrc.jp/research/db/TFSEARCH.html).

Real-time PCR quantification and protein detection

Total RNA was isolated from cells using Trizol reagent (Invitrogen). RNA quality was measured using A260/A280 readings. cDNA was synthesized and real-time PCR were conducted on a 7900 HT Fast Real Time PCR system (Life Technologies). The expression

level was calculated by using the difference of threshold cycle method (ΔCt) with normalization to the reference genes (RNU6B or GAPDH).

For proteins, intra-cellular proteins were detected by the western blot. Cells were homogenized in 100 μl of protein extraction reagent (Thermo Scientific, Waltham, MA, USA) and protease inhibitor (Panomics, Fremont, CA, USA). Protein concentration was determined by the Pierce BCA Protein Assay Kit (Thermo Scientific). Protein of 20 μg was loaded per lane and separated by NuPAGE Novex Bis-Tris 4-12 % mini gel electrophoresis (Invitrogen) in the Novex Xcell-II apparatus for 120 min at 100 V, and then transferred to Immbilon-PVDF transfer membranes (Millipore, Billerica, MA, USA) for immunoblotting. Proteins were visualized by enhanced chemiluminescence according to the manufacturer's instruction. Nonspecific binding was blocked with 5 % nonfat milk for 1 hour at the room temperature.

The antibodies to IKKα, IKKβ, IκBα, p-IκBα and β-actin were purchased from Genetex (Irvine, CA, USA). The antibodies to IκBβ and VCAM-1 were purchased from Abcam (Cambridge, MA, USA). The antibodies to p-IκBs was purchased from Cell Signaling (Danvers, MA, USA). The antibody to E-selectin was purchased from Biovision (Milpitas,CA. USA). The antibodies to ICAM-1, eNOS, CD40 and GAPDH were purchased from BD (Franklin Lakes, NJ, USA). For the NF-κB signaling, the nuclear proteins were extracted by the NucBuster protein extraction kit (Novagen, Madison, WI, USA). The

antibodies to p65, p50, p52, RelB and Lamin B were purchased from Santa Cruz Biotechnology (Santa Cruz, CA, USA). Tie-2 and anti-Ti2-P antibodies were purchased from Millipore (Bedford, MA, USA). Anti-body for POU2F1 was from Cell Signaling Technology (Danvers, MA, USA).

The proteins in the supernatant of culture medium were detected by the enzyme-linked immunosorbent assay (ELISA) kits (BD Bioscience, CA, USA).

Northern blotting assay for miR-195

The northern blot hybridization used the miRNA northern blot assay kit (Signosis, CA, USA). 5 μg total RNA was loaded to each well. RNA was fractionated using 15% denture gel, blotted on membranes, and hybridized with biotin labeled miR-195 and U6 probes.

Monocyte adhesion assay

THP-1 cells were suspended in medium with 5 μM of Calcein AM (C3100MP, Invitrogen). The Calcein AM–loaded THP-1 cells (200 μl at 5 x10^5 cells/ml) were added to the wells containing HUVECs. Non-adherent THP-1 cells were removed and fluorescence of adherent THP-1 cells was detected by a fluorescence microscope and the intensity of fluorescence was measured by a plate reader at 485 nm excitation and 515 nm emission filters.

Transfection of microRNA, siRNA and lentiviral-based short hairpin RNA (shRNA)

The sequences of synthetic miR-195 mimic, miR-195 inhibitor and NC-miR were 5’-UAGCAGCACAGAAAUAUUGGC-3’, 5’-GCCAATATTTCTGTGCTGCTA-3’ and 5’-AGUACUGCUUACGAUACGG-3’ respectively. The Lipofetamine 2000 (Thermo Fisher Scientific) or HiPerFect Transfection Reagent (Qiagen) was used for transfection. The lentivirus clone containing shRNA was obtained from the National RNAi Core Facility (Academia Sinica, Taiwan). shRNA plasmid (1μg /mL) or empty vector (pLKO.1 puro) was transfected to the cells using Lipofectamine 2000 (Invitrogen).

Viral-miR preparation

The DNA fragment encoding pre-miRNA-195 was amplified by PCR from human genomic DNA. The PCR primers were: forward-5'-AAGTGGAGTCTTTGTTGCCCACACCCAGCT-3' and reverse-5'-CCACCCT GCCTGGAGCAGCACAGCCAATAT-3'. The adenovirus expressing miR-195 (Ad-miR-195) and control adenovirus expressing GFP (Ad-GFP) were generated using the RAPAd miRNA Adenoviral Expression System kit (Cell biolabs, CA, USA) according to the manufacturer’s protocols. The inserted fragment was verified by automated sequencing. Ad-miR-195 and Ad-GFP were generated using the RAPAd miRNA Adenoviral Expression System kit (Cell biolabs, CA, USA).

For virus amplification, we infected the adenoviruses into HEK293A cells, and then purified the virus by ViraBind Adenovirus Miniprep kit (Cell biolabs) followed by titration with the QuickTiter Adenovirus Titer Immunoassay kit (Cell biolabs). Viral multiplicity of infection was estimated based on in vitro HEK-293A transduction efficiency: 0.5 ml of undiluted viral stocks was added to 10^6 HEK293A cells cultured in the 12-well plates, and number of GFP-positive cells was counted 48 h after transduction. After transfection for 48 hours, supernatants from virus-containing cell culture were harvested and deep frozen in aliquots.

Rat model for balloon injured carotid artery and stroke

The procedure for balloon injury can be found in our previous publication (Wang et al., 2012). For ischemic stroke model, male SD rats (280 to 350 g) were used for the induction of middle cerebral artery occlusion (MCAO) with previously reported surgical approaches (Candelario-Jalil et al., 2005; Wang et al., 2010). Rats were sedated with isoflurane (Abbott Laboratories Ltd., Queenborough, Kent, UK), anaesthetized by intraperitoneal administration of pentobarbital sodium (40 mg/kg; Sigma – Aldrich). A 3-0 nylon filament with silicon modification at the tip was inserted into a small nick on the right CCA and advanced approximately 22 mm beyond the carotid bifurcation to occlude blood flow to the middle carotid artery (MCA). Thereafter, surgical sutures were ligated along the CCA rostral to the nick to anchor the nylon filament and to seal off the vessel. The skin incision was

closed with surgical suture and topically treated with antibiotic ointment. For the permanent MCAO, the inserted nylon filament was left for 24hr and then the rats were sacrificed by over-dosed isoflurane at 24hr post-stroke because of high mortality and severe morbidity after 24hr MCAO. For transient MCAO, the inserted nylon filament was removed for reperfusion after 2hr occlusion. The rats subjected to transient MCAO were evaluated for the Garcia score and then sacrificed on day5 post-stroke.

For the hemorrhagic stroke, male SD rats (280-320 g) were sedated with isoflurane (Abbott Laboratories Ltd., Queenborough, Kent, UK), anaesthetized by intraperitoneal administration of pentobarbital sodium (40 mg/kg; Sigma–Aldrich), and then placed in a stereotaxic frame in a supine position on a warming pad at 37 °C. intracranial hemorrhage (ICH) was induced by stereotaxic infusion of bacterial collagenase Type IV-S (0.6 U in 1.0 μl sterile saline, Sigma-Aldrich) over a period of 5 minutes (0.2 mm posterior, 3.0 mm right, 6.0 mm depth to bregma at the skull surface). The needle was kept in place for another 10 minutes to prevent backflow. The ICH animals were sacrificed on day3 post-stroke.

miR-195 mimic (10 nmol/kg) or normal control microRNA (NC-miR) was formulated with In vivo-jetPEI® (PolyPlus Transfection Inc. IIIkirch, France) according to the manufacturer's instructions. Formulated microRNA was administrated intravenously (IV)

via tail vein after stroke induction. The treatment was given at 30 min, 3h, 4.5h and 6h for the permanent MCAO group, only 6h for the transient MCAO group, and 4h for the ICH group. The operators were blinded to treatment assignment of miR-195 or NC-miR.

The brains were collected and sliced into 2 mm coronal sections. The ischemic brain slices were stained with 0.1% 2,3,5-TTC. Stained brain slices were scanned with a flatbed scanner. Digital photographs of the brain slices were taken and lesion volume was computed using Image J (version 1.40, NIH, Bethesda, MD, USA). The total lesion volume or lesion percentage of brain (mm^3) was calculated as the sum of lesion area in each section.

Neurological score

Rats subjected to transient MCAO were evaluated for the Garcia score. To exclude potential failure of induced ischemic stroke, only rats with the Garcia score between 6 and 8 at 6h post-MCAO were included for the further studies. This neurological score will test for spontaneous activity, symmetry of movement and outstretch of limbs, circling behavior, climbing ability, body proprioception, and vibrissae touch. Each item was graded from 0-3 with the overall Garcia scores ranging from 0 to 18.

Similarly, to exclude potential failure of induced hemorrhagic stroke, rats were evaluated by the severity of movement impairment, and only impairment reached the moderate or severe

level, the rats were used for further studies. The movement evaluation has 3 grades – (1) “Mild” if a rat walked a straight line, weaker grip of the left forelimb and could stand on their own in a cage, (2) “Moderate” if a rat circled or walked to the left, activity was weakened and almost could not grip the left forelimb, and (3) “Severe” if a rat failed to walk without help, almost could not grip of the left forelimb and no activity.

The graders were blinded to treated and placebo groups. The assessment was performed on day3 and day5 for transient MCAO rats and on day1, 2 and 3 for ICH rats.

Assessment of brain edema

Because the brain edema peaked on day3 post-ICH (National Institute of Neurological and Stroke rt, 1995), the water content in the brain was measured using a common wet/dry method as previously described. On day3 the brain was removed to obtain the wet weight and the cerebellum was used as an internal control. The sample was then dried in an oven at 85°C for 48h to obtain the dry weight. The water content was expressed as a percentage of the wet weight: [(wet weight)-(dry weight)] (wet weight) $^{-1}$ × 100 %.

Evaluation of BBB permeability

Cerebrovascular permeability was assessed by a modified Evans blue extravasation method. On day3 post-ICH, rats were anesthetized and injected with 2% solution of Evans blue in normal saline (4 ml/kg of body weight) into the tail vein. The stain was allowed to circulate

for 2h. After that the rats were perfused with 300 ml normal PBS to wash out any remaining dye in the blood vessels and then the brains were removed and sectioned to 2 mm thickness. The cerebellum was used as an internal control. Evans blue dye was extracted by incubating them in N,N-dimethyl formamide overnight at 55°C and vortexed for 5 minutes. The mixture was subsequently cooled for 30 minutes and centrifuge (1500 g at 4°C) for another 30 minutes. The absorbance of Evans blue in the supernatant was then measured with a spectrophotometer at 610 nm. The results were presented as (g of Evans Blue stain) / (g of brain tissue).

Immunofluorescent staining and immunohistochemistry (IHC) staining

Immunofluorescent staining was used to detect cellular expression of Ang-1 (Sigma-Aldrich), COMP (Biorbyt), SDF-1 (Millipore), Sox2 (Abcam), Nestin (Abcam) and GAP43. IHC was used to stain the markers in brain slices. For brain slices, after 4% paraformaldehyde fixation for 15min, the slices were blocked in blocking buffer for 1 hour, incubated with primary anti-bodies overnight at 4℃, and followed by incubation with the secondary anti-bodies conjugated with anti-rabbit Alexa 488, anti-goat Alexa 647, or anti-mouse Alexa 647 for 1 hour. Nuclei staining was performed with 1ug/ml DAPI (Molecular Probes, Carlsbad, CA) for 5min at room temperature. After extensive washing, the coverslips were dried and mounted on glass slides.

Isolation and culture of neural stem cells

The tissue from SVZ was dissected, kept in 10 ml of ice-cold Hibernate A medium and cut into small pieces. After centrifugation, HBSS containing 0.1% (w/v) trypsin and 0.01% (w/v) DNase 1 was added, followed by rotation at 37°C for 60 min. Fetal bovine serum was used to stop the digestion, followed by centrifugation, and re-suspended in HBSS. The cell and tissue suspension was filtered and washed with the N2 medium. After removing excess myelin and other cell types, cells were seeded on fibronectin-coated culture plates in a plating medium (N2/DF), and maintained at 37°C in a humidified 5% CO_2 atmosphere.

Study approval

The Animal Care and Use Committee of the Kaohsiung Medical University approved the animal experimental protocols, which strictly conforms to the NIH Guide for the Care and Use of Laboratory Animals (NIH Publication No. 85-23, revised 1996).